Appendix E

Steam Dryer Structural Analysis Methodology

TABLE OF CONTENTS

Page

LIST OF TABLES

LIST OF FIGURES

Acronyms and Abbreviations

Acronym	Definition
ABWR	Advanced Boiling Water Reactor
ASME	American Society of Mechanical Engineers
B&PV	Boiler and Pressure Vessel
BWR	Boiling Water Reactor
DLF	Dynamic Load Factor
DOF	Degrees of Freedom
ESBWR	Economical Simplified Boiling Water Reactor
FE	Finite Element
FEM/FEA	Finite Element Model/Finite Element Analysis
FIV	Flow Induced Vibration
GEH	GE Hitachi Nuclear Energy
HCF	High Cycle Fatigue
HF	High Frequency
LF	Low Frequency
MASR	Minimum Alternating Stress Ratio
MPa	Mega Pascals
MSL	Main Steam Line
MSLB	Main Steam Line Break
PBLE	Plant Based Load Evaluation
PB	Bending Stress
PL	Local Primary Membrane Stress
PM	General Primary Membrane Stress
PT	Penetrant Testing
Q	Secondary Stress Range
RMS	Root-Mean-Square
RPV	Reactor Pressure Vessel
SI	Stress Intensity
SCF	Stress Concentration Factor
SRSS	Square Root of the Summed Squares

1.0 OVERVIEW

The purpose of this licensing topical report is to define the methodology used by GE Hitachi Nuclear Energy (GEH) for performing the structural analysis of steam dryers. This includes the analysis methodology for predicting the structural response of steam dryers to the flow induced vibration (FIV), the procedure for fatigue evaluation and the procedure for performing the primary structural analyses for load combinations at different service level conditions. The described fatigue evaluation and load combinations are consistent with the American Society of Mechanical Engineers Boiler and Pressure Vessel Code (ASME B&PV Code).

This Appendix is part of the overall methodology used by GEH to evaluate the steam dryer structural response under all service conditions. It belongs to a group of licensing topical reports that together define the methodology for evaluation of steam dryers. Each report covers certain aspects of the methodology. Appendix A, Steam Dryer Integrity Analysis Methodology, defines the overall steam dryer evaluation methodology, which covers plant and dryer instrumentation, load definition, structural analysis, limit curve development and power ascension monitoring. Appendices B, ESBWR Steam Dryer-Plant Based Load Evaluation Methodology, and C, ESBWR Steam Dryer-Plant Based Load Evaluation Methodology Supplement 1, define the acoustic-based Plant Based Load Evaluation (PBLE) - the GEH proprietary load definition methodology. This Appendix defines the subsequent structural analysis methodology applicable to all BWR steam dryers. Appendix D, GEH Boiling Water Reactor Steam Dryer-Plant Based Load Evaluation, provides the justification for the applicability of the ESBWR PBLE load definition methodology to all parallel bank BWR steam dryers used in the BWR/2 through BWR/6 and ABWR product lines.

2.0 STEAM DRYER DESCRIPTION

This section describes the design features of the typical BWR parallel bank steam dryer that are relevant to the dryer structural evaluation. Examples of finite element models are also provided.

The steam dryer is designed to remove the remaining liquid from the mixture of steam and water (wet steam) that exits upward from the steam separators. Wet steam enters the bottom of the dryer through inlet enclosures, flows horizontally through dryer vanes that remove the water droplets, and finally exits the dryer vertically through outlet areas into the dome of the reactor pressure vessel (RPV). The water removed from the steam is collected in troughs below the vanes and returned through the drain channels to the RPV water. Figure 2.0-1 shows the steam path and a schematic of the dryer bank. Figure 2.0-2 and Figure 2.0-3 provide an overall illustration of the main components of a steam dryer. The dryer skirt and hood panels direct the steam flow from the separators through the drying vanes. The support ring and troughs form the main support structure for the dryer. The support ring rests on four to six steam dryer support brackets that are welded attachments to the RPV wall. The dryer skirt is suspended from the support ring and extends below the water surface in the RPV in order to form a water seal around the steam separators.

The dryer vanes are vertically oriented chevron plates. Typically, 70 to 80 of these chevron-shaped vane plates are tied together by horizontal tie rods into a vane module or dryer unit. End plates provide support for the tie rods. Figure 2.0-4 shows top views of the vane module for both early and later model dryers. While the vane modules are not structural components, they represent a significant portion of the total mass of the dryer (on the order of 30-40%) and, therefore, the inertia effect is significant under most dynamic loading conditions.

The significant steam dryer structural components are shown in Figure 2.0-2 and Figure 2.0-3. Multiple vane modules are aligned longitudinally to form a dryer bank. The dryer bank assembly consists of the vane modules, the drain trough, and the hood panels that form the inlet plenum to the dryer vane bundles. Four to six parallel dryer banks are used, depending on the size of the dryer. BWR/4 and later dryer designs incorporate interior vertical hood support plates to provide structural support and break up lower vibration modes of the large hood span. These interior support plates abut the end plates of the vane modules. On the hood side of the support plate, some designs incorporate a backing strip between the support plate and hood plates. This backing strip provides additional support at this critical junction. Additional horizontal plates attached to the support ring are used to close off steam flow paths between the banks. Vertical plates are attached at the ends of the banks to form an outlet plenum between banks. These plates direct the steam flow exiting the banks upward into the steam dome region.

The support ring, along with the drain troughs, forms the foundation of the dryer. The dryer bank assemblies are welded to the top of the support ring. On some dryer designs, cross beams attached to the support ring provide additional support to the troughs. Bank-to-bank tie bars on the top of the dryer provide structural support across the top of the dryer.

The support ring rests on four to six steam dryer support brackets that are welded attachments to the RPV wall. Seismic blocks are attached to the support ring at each of the bracket locations. The motion of the steam dryer in the circumferential direction is constrained by the seismic blocks, while leaving the support free in the radial direction to accommodate differential thermal expansion between the dryer and the RPV.

The dryer skirt is suspended from the support ring. A number of panels are welded to the inside of the skirt (BWR/2-3 designs) or the outside of the skirt (BWR/4 and later designs) to form the drain channels. Pipes connect the troughs to the drain channels to provide a flow path for the water removed from the steam by the vanes. Welded to the bottom of the skirt is the lower skirt ring. During refueling, the dryer rests on the lower skirt ring in the equipment pool.

GEH BWR steam dryer technology has evolved over many years and several product lines. In earlier BWR/2 and BWR/3 dryers, the typical active height of the dryer vanes is 48 inches. Vane material typically extends about 1.5 inches above and 3 inches below the active vane height. This inactive height of vane material is physically captured and supported by the bank assembly. Some BWR/2 GEH steam dryers inclined the dryer units 20° from vertical; however, later GEH BWR steam dryers install the units vertically. In BWR 4/5 steam dryers the active vane height was increased to 72 inches. The higher vanes have been carried into later product lines. Figure 2.0-5 illustrates the evolution of steam dryer banks and terminology used for the hood types. BWR/2 and BWR/3 plants used square hood dryers. It should be noted that the square hood dryers from only one fabricator incorporated internal diagonal braces. The slanted hood design was introduced with the BWR/4 product line. The curved hood design was introduced with the BWR/5 product line and has been used in subsequent plant designs. The curved hood dryer was also used in several later BWR/4 plants. These differences in hood designs affect the dryer modal response. Perforated plates are included on the inlet and outlet sides of the vanes of 72-inch height units in order to more effectively utilize the increased vane height. The addition of perforated plates results in a more uniform velocity over the height of the vanes. While not intended to be a structural component, the perforated plates do add stiffness to the dryer bank assembly.

The same basic GEH BWR steam dryer design has been used in BWR/2 through BWR/6, ABWR, and ESBWR product lines. This basic design consists of four to six parallel banks supported by a circumferential ring at about mid height of the dryer. The banks consist of hood

panels that direct the steam flow through the dryer vane assemblies. The skirt is suspended from the support ring and extends down below the reactor water level and outside the steam separator assembly. The skirt forms a water seal and directs the steam leaving the separators up through the vanes. Water removed from the steam is collected in troughs below the vane assemblies and returned to the RPV water through the drain channels. The evolutionary design of the BWR plants resulted in many similar configurations in addition to the parallel bank dryer design (Appendix D). Therefore, the discussions in this licensing topical report apply to all GEH BWR dryers.

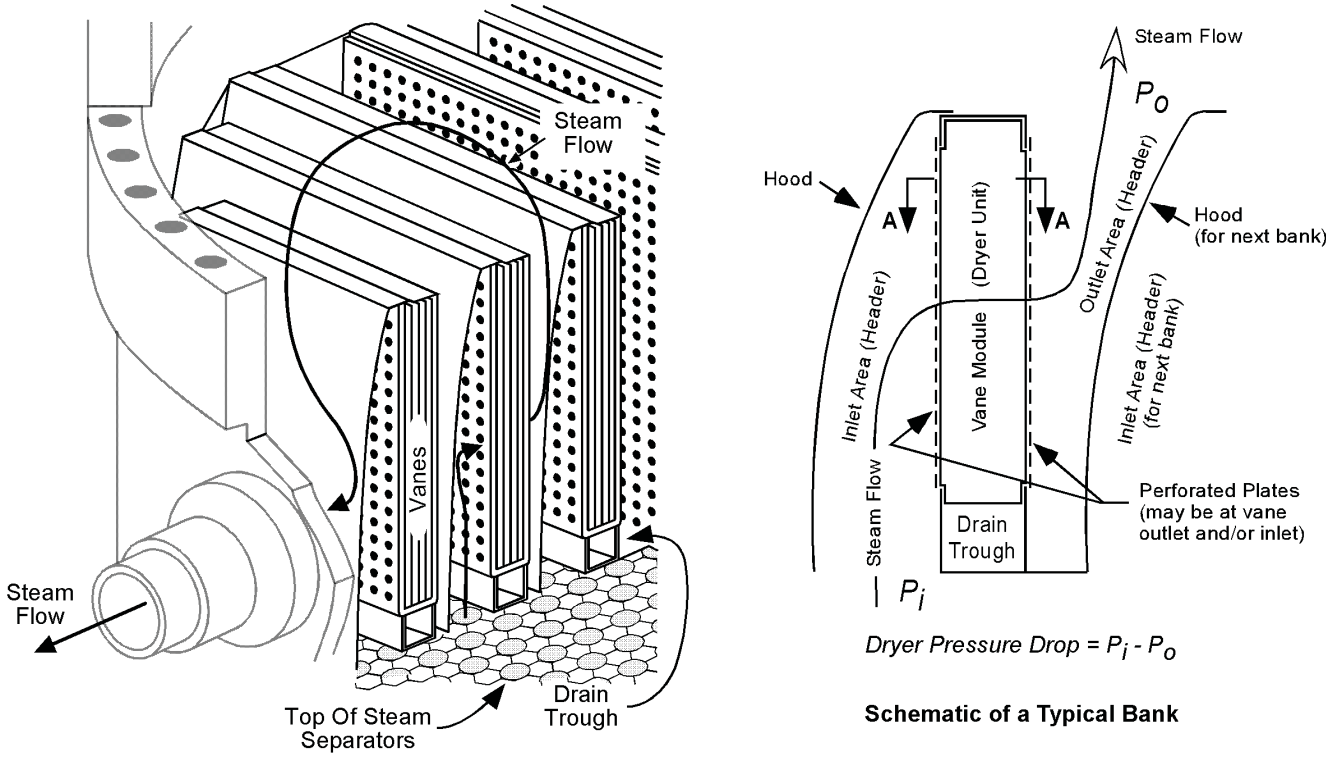

Figure 2.0-1 Steam Flow Path and Partial Dryer Profile

[[

]]

Figure 2.0-2 Structurally Significant Dryer Components

[[

]]

Figure 2.0-3 Structurally Significant Dryer Components

BWR/2/3 and 48” High BWR/4

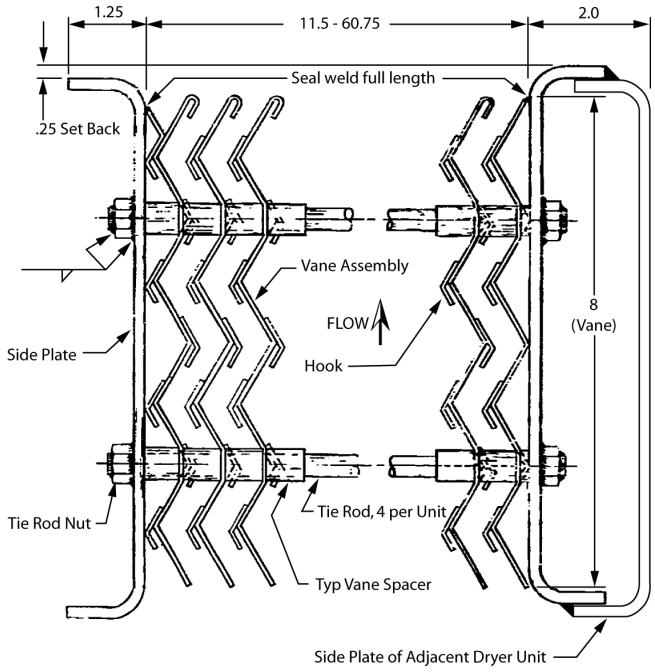

72” High BWR/4 and Later

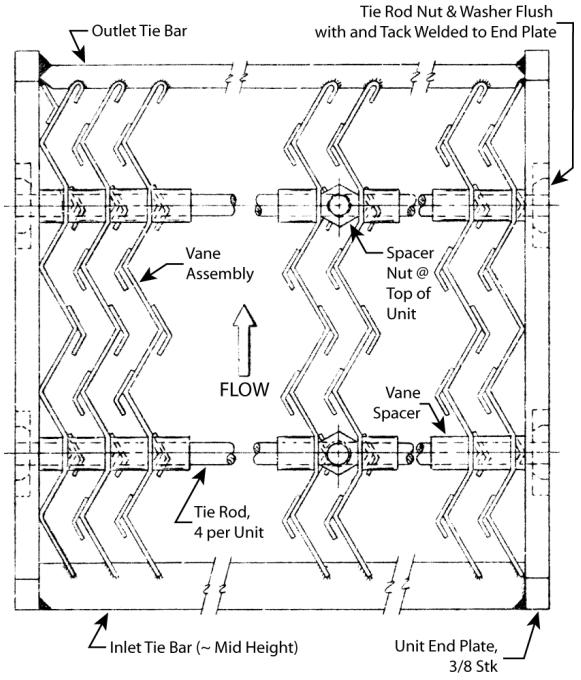

Figure 2.0-4 Schematics of Vane Modules

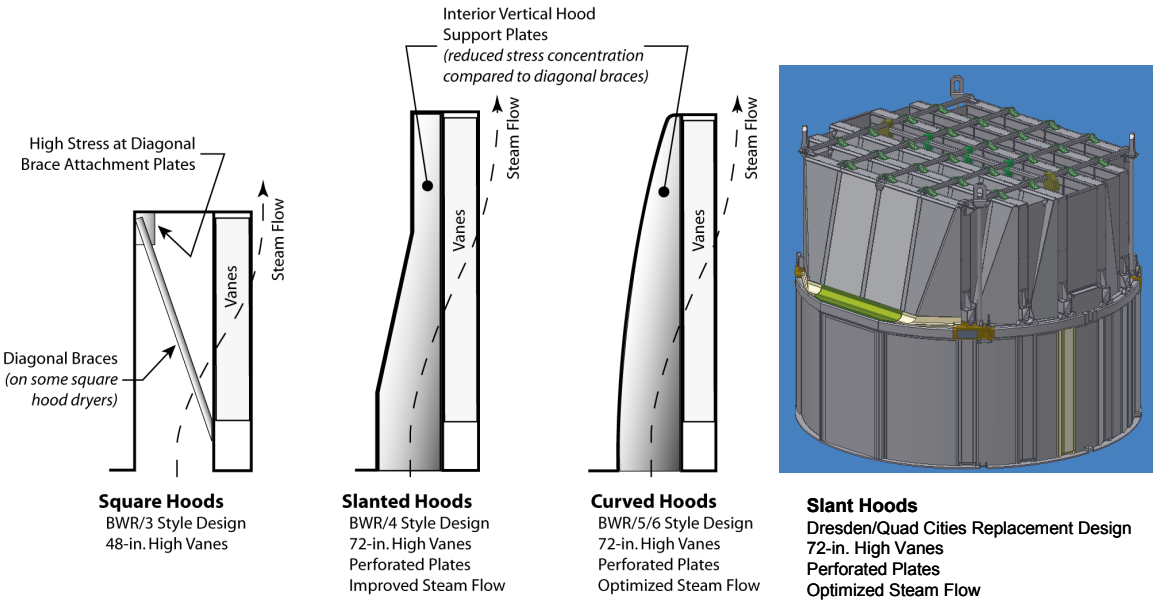

Figure 2.0-5 BWR Dryer Hood Designs

3.0 MATERIAL PROPERTIES

This section provides the guideline for the material properties used in the steam dryer structural analysis.

BWR steam dryers are manufactured from Austenitic 300 series stainless steel conforming to the GEH material and fabrication specifications. The grade most commonly used is Type 304. Recent replacement stream dryers use low carbon grade 304L to provide resistance to stress corrosion cracking. Material properties are obtained from the ASME B&PV Code (Reference 1). Steam dryers are operated at the steam saturation temperature corresponding to the RPV dome pressure. The elastic modulus of the steam dryer material will be reduced at elevated temperatures compared to that at room temperature. Specific material properties at the normal operating temperature should be used in analysis (e.g., 550°F for a dome pressure of 1045 psia). The applicable material properties from Reference 1 are shown in Table 3.0-1 below:

Table 3.0-1 Properties of SS304/SS304L at 550°F

Material/Property	Value at Operating Temperature
SS304/SS304L	
S_y, Yield Strength, psi	15,950
S_u, Ultimate Strength, psi	57,200
E, Elastic Modulus, psi	25.6×10^6

In addition, materials with properties different than the original dryer specification may have been used in modifications and repairs made to the dryer. The original material selection and repair/modification history of the individual dryer will be reviewed and the appropriate material properties for the affected components will be used in analysis.

4.0 DESIGN CRITERIA

The steam dryer, including the dryer units, is a GEH safety related item and is classified as an Internal Structure as defined in Reference 1, Subsection NG, Paragraph NG-1122. The steam dryer is not an ASME Code component, but the structural evaluation methodology uses the Code as a design guide with the exception of the weld quality and fatigue factors as discussed in Subsections 4.2.1 and 7.

4.1 FATIGUE CRITERION

The steam dryer structural analyses are performed assuming that the dryer will be operated for 40 to 60 years. The stresses are expected to be well within the elastic range when the dryer is subjected to FIV loading during normal operation. Therefore, the high cycle fatigue (HCF) life is the major design consideration. The fatigue stress limit is lower than the material yield stress. Steam dryer components are subjected to cyclic acoustic pressure in normal operation where high cycle fatigue constitutes the controlling structural acceptance criterion for steam dryers. Determination of the fatigue stress limit used in the FIV structural analysis is consistent with ASME B&PV Code Section III.

The design fatigue curves and curve selection criteria for Austenitic Ni-Cr stainless steel, the group of materials used for steam dryer, are given in the ASME code (Section III, Division 1, Appendix I, Figure I-9.2.2 and Figure I-9.2.3). The ASME stress-cycle, or S-N curves plot the alternating stress intensity versus number of cycles. Alternating stress limit is dependent on mean stress. [[

]] Curve C is the most conservative of the three curves in Figure I-9.2.2 and may be used at or near the weld locations where high residual stresses may be present. Curve C also includes margin to address the residual stress from fabrication. [[

]]

4.2 WELD FACTOR

A key component of the fatigue alternating stress calculation at a specific location is the appropriate value of the stress concentration factor (SCF). The weld types of relevance for the steam dryer stress analysis are the full penetration welds and fillet welds. [[

]]

For the case of NG-3352 Type I and III full penetration welded joints, [[

]]

For the case of a fillet weld, there are two distinct analysis paths depending on whether the stress was obtained from a shell element or a solid element model. [[

]]

The following describes the process of determining nominal stress near the weld for the shell model. [[

]]

The stress may also be obtained from the shell finite element model peak stress intensities obtained from time history analysis. Because the shell finite element model of the full steam dryer is not capable of predicting the full stress concentrations in fillet welds, weld fatigue factors, and if necessary weld size reduction factors, for fillet welds are applied to the calculated peak stress intensities to determine the fatigue stress.

The weld size reduction factor may be needed as stated above. When using the traditional Strength of Materials formulas, the effective weld size is taken into account in the weld section properties. [[

]]

If the shell model is not capable of determining the peak stress for the fillet weld then a solid submodel of the fillet weld region is created. In other words, this approach is used when the global shell model is inadequate to resolve the load path in small local regions of the steam dryer. These regions are typically places with small discontinuities in the structure where the coarser shell model or even a more refined shell model cannot adequately provide the proper local load path. [[

]]

The guidance above is based on Section III, Subsections NG and NB, of the ASME BP&V Code (Reference 1). The approaches of applying SCFs to shell and solid models described above are applicable to both bending and membrane stresses. The recommended SCF of 4 for the fillet welds is what has been recommended as the fatigue factor 'f' in Table NG-3352-1 of ASME Section III, Sub-section NG, for fillet welds. In recommending the use of this fatigue factor, Paragraph NG-3352 does not make a distinction in terms of the applicable stress types that is whether it is membrane, bending or combination of both.

The similar weld factor value for fillet welds can be derived using two sub factors: the first sub-factor (equivalent to C index in the piping fatigue stress analyses) accounts for the increase in the through-section stress over and above the nominal stress away from the weld discontinuity, and the second sub-factor (equivalent to K index in the piping fatigue stress analyses) accounts for the root discontinuities at the weld itself. [[

]] 1.8 is the maximum specified value of K index in Table NB-3681(a)-1 (i.e. for as-welded girth butt welds). Table NB-3681(a)-1 provides K index 1.2 for stress due to internal pressure, 1.8 for stress due to moment loading and 1.7 for stress due to thermal loading. [[

]]

4.2.1 Weld Quality Factor

For the case of the steam dryer, which is not a core support structure, it was judged that the use of ASME Boiler and Pressure Vessel Code Subsection NG weld quality factors needed to be further evaluated. Weld quality factors are used in the Code to assure adequate margin for static loading. For design against fatigue, margin is maintained by ensuring that the assumed loading is conservative and in the selection of the most conservative fatigue design criterion. The weld

quality factor is used in the Code to reduce the allowable stress limit based on the weld inspection method. Paragraph NG-3352 of the Code states that "the use of weld quality factor *n* is for static, not fatigue applications." The same Paragraph also states that "in performing a fatigue analysis, use the fatigue factor *f*, designated in Table NG-3352-1, and the applicable fatigue curve in Table I-9.0." The referenced fatigue factor *f* is equivalent to the weld factor or SCF in Section 4.2. [[

]]

To assure high quality welds, new or replacement steam dryer fabrication employs weld processes that have been fully qualified. Additionally, root and final penetrant testing (PT) inspections are required. When both sides of the weld are accessible, penetrant test nondestructive evaluations are effective at assuring surface imperfections or discontinuities do not exceed required limitations on the root and face of the weld. Limiting surface discontinuities is of particular importance to structures subject to fatigue. Where the root side of the weld is not easily inspected, such as fillet welds, partial penetration welds and some full penetration welds, robust weld process qualifications are conducted to prevent weld defects from occurring during fabrication. Representative weld samples using the same joint design and material types as specified for the new or replacement steam dryer are destructively tested. Metallurgical evaluations demonstrating an acceptable weld root are required prior to weld procedure approval. These tests demonstrate that no defects are present at the root of production welds.

[[

]]

[[

]]

Figure 4.2-1 Weld (Fatigue) Factor Flow Diagram

4.3 ASME CODE STRESS LIMITS FOR LOAD COMBINATIONS

The ASME Code stress limits from Subsection NG of Reference 1 are listed in Table 4.3-1.

Table 4.3-1 ASME Code Stress Limits

Service level	Stress category	Core Support Structures Stress limits (NG)
Service Levels A&B	P_m	S_m
	$P_m + P_b$	$1.5S_m$
Service Level C	P_m	$1.5S_m$
	$P_m + P_b$	$2.25S_m$
Service Level D	P_m	$\text{Min}(0.7S_u \text{ or } 2.4\ S_m)$
	$P_m + P_b$	$1.5(P_m \text{ Allowable})$

Legend:

P_m:General primary membrane stress intensity
P_b:Primary bending stress intensity
S_m:ASME Code Design Stress Intensity
S_U:Ultimate strength

Note: Service Level Limits for Service Levels A, B and C are according to NG-3221 and for Service level D guidance is obtained from Appendix F Paragraph F-1331. Upset condition stress limits are increased by 10% above the limits shown in these table per NG-3223(a).

5.0 STEAM DRYER FEA MODEL AND APPLIED LOADS

A typical steam dryer and its structurally significant components have been described in Section 2.1. These components are included in the full steam dryer finite element model. The commercial finite element software ANSYS is used for the analyses. Section 5.1 provides the detailed descriptions of the finite element model. Section 5.2 describes the dynamic loading used for the fatigue evaluation. Section 5.3 describes the loads applied for the ASME Code evaluations.

5.1 FULL STEAM DRYER FINITE ELEMENT MODEL

A three-dimensional finite element model (FEM) of the steam dryer based on nominal dimensions is created using the ANSYS finite element code (Reference 2). The global FEM models all the structurally significant components of the dryer. The model consists predominantly of shell elements, [[

]] where appropriate. The model also includes the water to structure interactions for the submerged portion of the skirt. [[

]]

5.1.1 Elements and Model Simplifications

The commercial finite element software ANSYS is used in the steam dryer analysis. The finite element model of the steam dryer contains predominantly shell elements. Each node on the shell element has six degrees of freedom – three translational and three rotational. This type of shell element is of elastic formulation and allows both bending and membrane stresses. Three in-plane stress components as well as an out-of-plane normal stress are permitted. ANSYS defines three layers through the shell element thickness (i.e. top, middle and bottom layer). Locations of these layers are determined by the normal orientation of the shell element and stresses can be calculated on these layers. For the FIV analysis, stresses are evaluated and scoped for both top and bottom layers.

Besides the shell element, other types of elements are also used in dryer models. [[

]] Section 5.1.2 discusses the confirmation of the mesh convergence for the model.

Certain simplifications are made when creating a dryer model. These simplifications are made in part to maintain a reasonable model size and analysis run time. These simplifications do not sacrifice the accuracy of the overall structural response of a modeled dryer. The simplifications are explained below.

[[

]] Treatment of welds in analysis has been discussed in the light of weld factor in Section 4.2. Submodeling is discussed in Section 6.2.2.

[[

]] This modeling is further discussed in Section 5.1.5.

[[

]]

Figure 5.1-1 An Example of Steam Dryer Finite Element Model

5.1.2 Mesh Size and Mesh Sensitivity

If the finite element model mesh is not refined enough, the analysis results may be nonconservative. To determine the adequacy of the mesh, a mesh convergence study is performed. [[

]]

Table 5.1-1 Typical Mesh Size: Global FE Dryer Model

[[

]]

5.1.3 Dryer Vane Bundle Model

An overall description of the dryer vane bank has been provided in Section 2.0. A vane bank consists of multiple vane modules. Vane bundles are vane modules without end plates. Each vane bundle contains numerous chevron-shaped vanes as well as tie rods and support pads. The construction of a GEH vane bundle is shown in Figure 5.1-2 and Figure 2.0-4.

The vane modules make up a large part of the total mass of a dryer (Section 2.0). [[

]]

A global dryer FEM contains the degrees of freedom (DOF) used directly in the FIV analysis for a full dryer. [[

]]

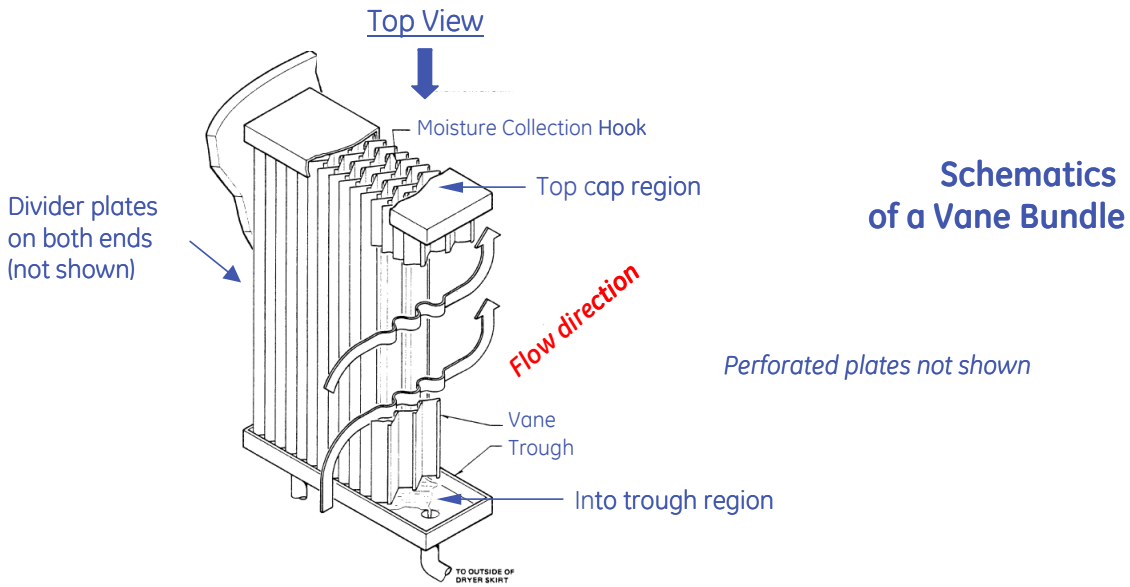

Figure 5.1-2 Vane Bundle Construction

[[

]]

Figure 5.1-3 Vane Bundle FEM and Master DOFs

5.1.4 Water Modeling

The water to structure interaction is included for the submerged portions of the steam dryer. The bottom half of the dryer skirt is submerged in the water. The water provides a resisting pressure on the skirt/drain channel panels as they vibrate through water, having being excited by the oscillating acoustic pressure. These fluid-structure interactions are manifested in the fluid resistance to the structural vibration and may significantly alter the dynamic response of the entire steam dryer.

Water inside and outside skirt is simulated in the structural finite element model. The water levels on the top of the modeled regions are different between inside and outside the skirt. The top surface of water level outside skirt is set at the RPV water level during normal operation. The top water level inside skirt is lower by the equivalent static head of the pressure drop of the steam flow through the vane banks. The bottom water level is determined from the bottom level of steam separator. The bottom of water typically extends below the lower skirt ring.

The outer diameter of the water model is equal to the reactor vessel inner diameter. The inner diameter of the water model is equal to the minimum diameter of an inner circle containing all the steam separator tubes. Water movement is unobstructed within the annular belts between skirt and the separators, and between skirt and the vessel wall. Thus, the modeled water is annular in shape with two stepped levels as shown in Figure 5.1-4. The outer level (higher step) represents the water outside skirt and the inner level (lower step) represents the water inside skirt.

[[

]]

The displacement boundary conditions are applied to the water model in the following manner. All nodes from the water model that are located on the surface of water outer or inner diameter are fixed only in the radial direction, representing the solid boundary of either the reactor vessel

wall or steam separator. Most nodes on the bottom of the modeled water are fixed in the reactor axial direction.

The water surrounding the skirt and drain channels contains a large number of steam bubbles from the steam entrained in the separator spillover flow. This bubbly water is modeled in the fluid elements. The bubbly water properties are significantly different than those of solid water because of the presence of steam bubbles. The carry-under fraction (the mass fraction of the *wet* steam in the mixture of water and bubbles) is used to determine the characteristics of the bubbly water mixture. [[

]] Figure 5.1-5 shows a schematic of *carry-under* as well as the steam-bubbly water interfaces. Further discussions of the effects of the bubbly water on the dryer analyses can be found in Appendices B and C.

Density and bulk modulus are the two major properties required for the ANSYS fluid elements in the model. The bulk modulus measures the resistance to uniform compression, namely, the volumetric deformation under pressure. It also defines the compressive sound wave in fluids and is a significant parameter in determining the sound speed in a fluid medium.

The following is the general equation used to calculate the density of the mixture of fluids. It applies to the density of bubbly water as well as the density of wet steam. If the mixture is bubbly water, the density of the entrapped wet steam is used for ρ_{steam} in the equation. If the mixture is wet steam, the density of dry steam should be used instead. Such dry steam is the compressed steam in the BWR environment of elevated temperature and pressure.

$$\rho_{mixture} = \frac{1}{\frac{q}{\rho_{steam}} + \frac{1-q}{\rho_{water}}} \qquad (5.1\text{-}1)$$

where

$\rho_{mixture}$ = Density of mixture, e.g., the bubbly water or wet steam.

ρ_{steam} = Density of wet or dry steam.

ρ_{water} = Density of the saturated water in a typical BWR RPV environment.

q = Steam quality. If the mixture is bubbly water, q will be carry-under fraction.

For downstream wet steam, the steam quality q is over 99.9% and 1-q is almost zero. Substituting them into Equation (5.1-1), the density of wet steam ($\rho_{mixture}$ in the equation) is found nearly identical with the density of compressed dry steam (ρ_{steam}). Appendix B provides the density of the saturated water in a typical BWR RPV environment (approximately 550^{o}F), which is about 0.026~0.027 lbs/in^{3}. This value is significantly lower than that of water at ambient temperature. Appendix B also provides the density of the typical wet steam found in a BWR RPV environment. Its value is approximately 0.0013 lbs/in^{3}. Equation (5.1-1) is then applied once again to obtain the density of bubbly water using those of the saturated water and wet steam.

Derived from the wave equation, the speed of sound in the bubbly water is related to the density and bulk modulus of the bubbly water. The relation may be expressed in the following equation,

[[ ]] (5.1-2)

Where:

[[

]]

The speed of sound within the bubbly water in the typical BWR RPV of elevated temperature and pressure (approximately 550^{o}F and 1050 psi) is obtained from the curves in Figure 12 of Appendix B. [[

]] For dryers with significantly different carry-under fraction and operation conditions, those parameters should be re-calculated using the above equations and relevant data. The bulk modulus of the bubbly water in a typical BWR RPV environment is less than one thousandth of the bulk modulus of pure water at ambient temperature. Bubbly water provides less resistance than solid water to the vibration of the submerged skirt and drain channels.

[[

]]

Figure 5.1-4 Modeling Water

[[

]]

Figure 5.1-5 Schematics of Bubbly Water and Steam

5.1.5 Perforated Plate

In BWR/4 and later dryers, vane bundles are enclosed by perforated plates on each side. The small holes in the perforated plates distribute the steam uniformly over the height of the vane bank. These openings will reduce the mass and stiffness of the plate compared to a plain plate without openings.

A large perforated plate attached to one side of a dryer bank is made of multiple rectangular smaller plates. The perforated plates are welded around their periphery to the top caps, vane module end plates, and trough to provide a steam seal. As a result, the perforated plates provide a direct load path from top caps to the troughs. They also interact with the hoods through hood supports and vane module end plates. In addition, these perforated plates carry significant amount of weight due to their large area despite the fact that they are typically only 1/8" thick. Perforated plates have both inertia and stiffness effects on the FIV response.

[[

]]

[[

]]

Figure 5.1-6 Modeling Perforated Plates

5.1.6 Submodel

Submodeling of high stress regions becomes necessary if the relatively coarse global model is not considered adequate enough to resolve the stress, or if the stress is significantly affected by the local features not modeled in the global model. Section 6.2.2 provides the details on the steam dryer-related submodeling including modeling requirement, analysis procedure and post processing of stresses.

5.2 DYNAMIC LOADS

5.2.1 FIV Pressure Loads

The driving force in the FIV structural analysis is the oscillating acoustic pressure generated by the steam flow inside the reactor dome and four main steam lines (MSL). The FIV load definition is generated based on measurements from on-dryer pressure transducers or pressure measurements taken on the MSLs (typically using strain gages to measure the pipe hoop stress). The PBLE methodology (Appendices B and C) is used to determine the acoustic pressures acting on the dryer from the plant measurements. [[

]] so that the FIV loads determined by the stress analysis will have considered the peak stress intensities that occur at frequencies as low as 1 cycle per 100 seconds. Events that occur less frequently are expected to have a diminished contribution to the FIV fatigue life. The process for selecting the analysis time interval and determining the time interval bias is described in Section 5.2.4. The solved acoustic pressures are then mapped and applied to the structural model to determine the forced response of the steam dryer. Figure 5.2-1 shows the flow chart of the acoustic pressure load definition process leading to the FIV structural analysis. The process for acquiring the plant measurements and developing the plant-specific FIV load definition is provided in Appendix A.

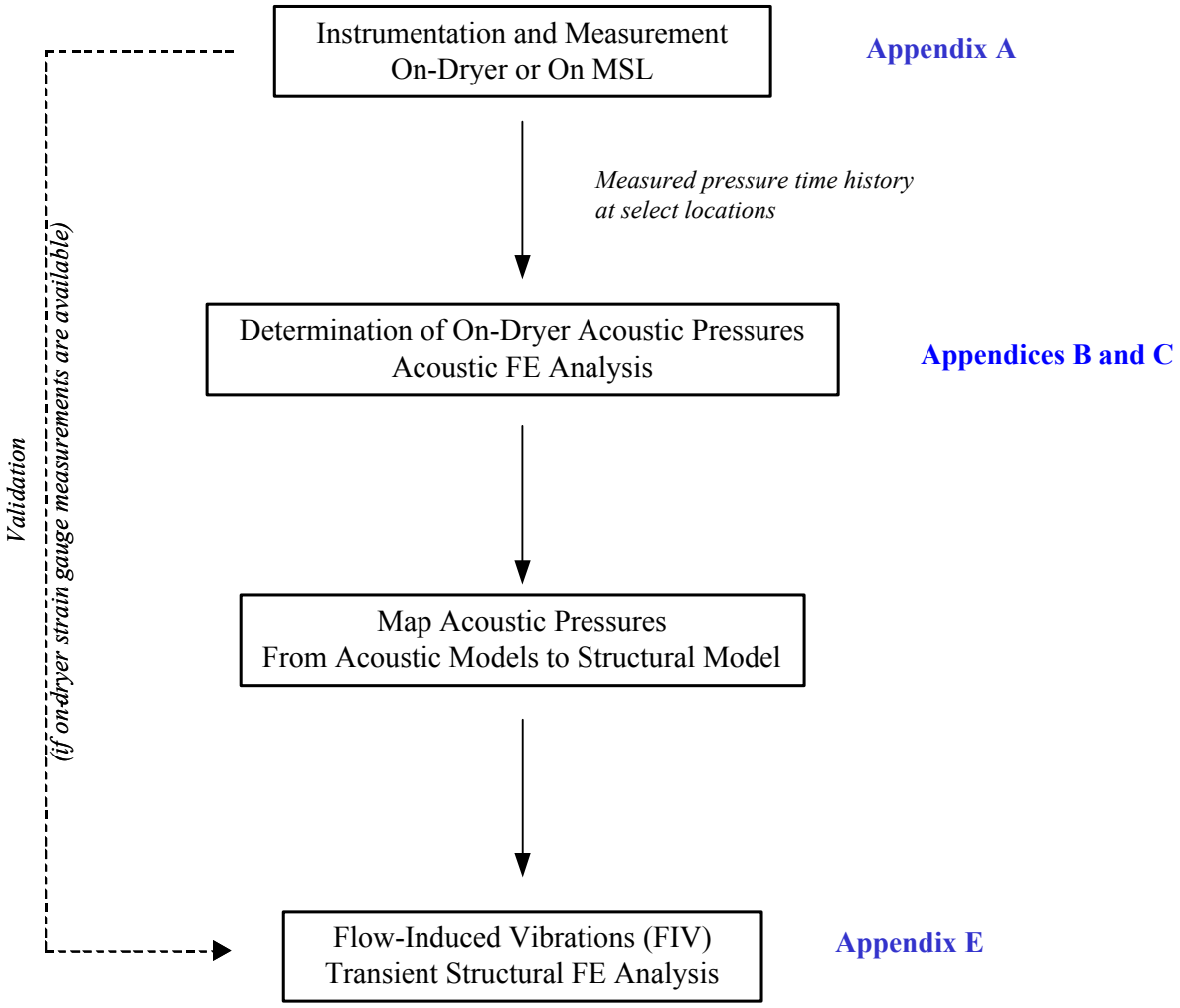

Figure 5.2-1 Process of the FIV Analysis

The acoustic finite element analysis is conducted in the frequency domain. The structural finite element analysis is performed in the time domain (Section 6.1). To apply the acoustic loads to the structural analysis, the acoustic pressure spectra of a steam dryer obtained from an acoustic analysis in the frequency domain have to be transformed first into the time history representations of acoustic pressures in the time domain at the respective locations. There are acoustic pressures on both sides of the dryer panels. The pressures on each side of the panel are resolved into a differential pressure, which is then applied as a pressure force to the structural model.

Typically, the mesh (in the form of nodes and elements) of the acoustic FEM does not match the mesh of the corresponding structural FEM. From an acoustic analysis in the frequency domain, acoustic pressures are evaluated at the acoustic nodes associated with the steam dryer pressure surfaces and then transformed to the form of nodal pressure force time histories. In order to map the acoustic pressures onto a structural model, the mesh from the structural model is first overlaid with the nodes from the corresponding part of the acoustic model (i.e. the acoustic nodes on the steam dryer surfaces). The pressure value of a structural node at each time step is then extracted from that of the acoustic node closest to it at the same time step. Pressures at all structural nodes are mapped in the same manner. This process is repeated for all time steps.
[[

]]

[[

]]

Figure 5.2-2 Contours of Evaluated and Mapped Acoustic Pressures

5.2.2 Bias and Uncertainty of the Steam Dryer FIV Stress

The bias and uncertainty error in the FIV structural analysis comes from various sources. There are uncertainties in the predicted dynamic response and structural modes of the steam dryer, owing to the approximations in the structural model and the uncertainties in the as-fabricated structure. [[

]] Section 8 of Appendix A provides a detailed description of the bias and uncertainty terms for the analysis process.

5.2.3 Dynamic Testing for Prototype Dryers

On a new plant or a prototype replacement dryer where there is more time and space to accommodate frequency response testing, shaker testing may be used in lieu of hammer testing. Either a hammer or a shaker with a force transducer will provide the excitation. Hammer or shaker testing is not practical on an irradiated dryer; however, the bias and uncertainty estimates based on the comparison of simulations and measurements taken on new dryers are applicable to operating dryers because the dryer construction is similar.

The excitation is applied at different accessible regions of the dryer: banks, skirt, end plates, and top caps. [[

(5.2-1)

]] The bias error is represented by frequency band and component. The bias and uncertainty is represented by the average and standard deviation of the error based on multiple tests for a dryer region.

5.2.4 Period of Peak Response for FIV Assessment

The FIV loading used in the finite element stress analysis considers peak stress intensities that occur at frequencies as low as ~1 cycle per 100 seconds. [[

]]

For direct integration structural finite element analysis, to achieve better low and high frequency response resolution while maintaining storage within supercomputer capacity, separate low and high frequency analyses are typically performed. [[

]]

In the F-Factor method, [[

(5.2-2)

(5.2-3)

]] (5.2-4)

This process is repeated over each of the frequency bands to generate the peak stress contribution from each band, Sn.

[[

]]

Table 5.2-1 Time Domain Strain Gage Data Statistics

[[

]]

Assume that [[

. (5.2-5)

. (5.2-6)

. (5.2-7)

(5.2-8)

(5.2-9)

(5.2-10)

(5.2-11)

(5.2-12)

(5.2-13)

]]

5.2.5 Bias and Uncertainty and Benchmarking Using Harmonic FE FIV Solution

The FE benchmark performed in Reference 3 was performed using an ANSYS solution with the direct integration method. If the ANSYS harmonic method is used for the dryer analysis, the

harmonic analysis and associated post processing is also benchmarked against test data and with the direct integration method results. The benchmarking will compare the predicted dryer response against test data and the harmonic stress predictions are compared against direct integration methods to demonstrate that the harmonic post processing methodology successfully identifies maximum stress regions of steam dryer subcomponents. The FE harmonic model bias and uncertainty is determined based on these benchmark comparisons.

5.3 ASME LOADS

Section 8 provides the detailed information on the load combinations assumed for the ASME B&PV Code analyses. The process for defining the various ASME load terms is provided in Appendix A.

6.0 VIBRATION ANALYSIS AND PREDICTED COMPONENT STRESSES

This section describes the process used to perform the FIV structural analysis. The commercial finite element software ANSYS is used in the solution. For the flow-induced vibration of steam dryers, GEH applies the ANSYS transient dynamic analysis (i.e. direct integration method) in the time domain with [[

]].

6.1 DYNAMIC ANALYSIS APPROACH

6.1.1 Structural Damping

Structural damping exists in steam dryers, which dissipates part of the vibration energy. [[

]] consistent with the recommendation in the USNRC Regulatory Guide 1.20 Revision 3.

Rayleigh damping is assumed and applied to all structural finite element models of steam dryers. Rayleigh damping assumes that damping matrix (**C**) is a *linear combination* of mass matrix (**M**) and stiffness matrix (**K**) in the equation of motion; namely,

$$\mathbf{C} = \alpha \mathbf{M} + \beta \mathbf{K} \qquad (6.1\text{-}1)$$

Where α and β are the alpha and beta Rayleigh damping constants.

[[

]]

[[ ]] (6.1-2)

Therefore, the damping ratio, i.e. the ratio of the damping constant over critical damping constant, varies [[ ]]. On a curve of damping ratio *versus* frequency, no more than two frequencies can have the same damping ratio. [[

]]

[[ ]] (6.1-3)

The Rayleigh damping ratio as described is frequency dependent if the alpha and beta damping constants are invariant. A constant damping ratio is prescribed at the anchoring frequencies ω_1 and ω_2. [[

]] damping ratio (ζ) for the structural analysis is assumed in the dryer analyses. In the time domain transient dynamic analysis with ANSYS, frequency-dependent and material-dependent alpha and beta damping constants cannot be defined and therefore, it is not possible to enforce the same damping ratio at all frequencies. As a result, two anchoring frequencies have to be selected [[ ]]. The anchoring frequencies are defined by the frequency range where significant pressure loads are present. This is to ensure that within the analyzed frequency range, the damping ratio is [[ ]] for the frequencies at which the structure is being driven.

In the typical dryer structural analysis, a wide range of frequency is covered. As shown by Curve 2 of Figure 6.1-1, a single damping curve covering the entire frequency range results in an effective damping ratio of much less than [[ ]] over a large portion of the frequency range. Thus, depending on the measured frequency content in the acoustic loads, [[ ]] structural analyses may be performed, each with its own governing damping curve. Curve 1 of Figure 6.1-1 shows [[

]]

The damping used for harmonic analyses in the frequency domain does not have the limitations imposed by Rayleigh damping in the time domain. A harmonic analysis in the frequency domain permits frequency-dependent damping ratios to be used. Harmonic analyses in the frequency domain will use a [[ ]] applied for all frequencies.

[[

]]

Figure 6.1-1 [[ ]]

6.1.2 Dynamic FIV Analysis

The commercial finite element software ANSYS is used in the FIV analysis for the steam dryer. The time domain full transient dynamic analysis method (transient analysis type and full solution method) in ANSYS is used for the structural analysis. This analysis employs direct integration over the time domain and therefore, it is also referred to as the direct integration method. Alternately, the harmonic analysis method in ANSYS may be used. Linear elastic analysis is performed for the FIV analyses because all the dryer materials are expected to remain within the linear elastic range during normal operation and there is no large nonlinear deformation involved.

The acoustic pressure load definition process is described in Section 5.2.1. The process for selecting the analysis time segment and determining the residual time segment bias is described in Section 5.2.4. The acoustic loads are periodic and contain a full spectrum of frequencies. In the time domain analysis, multiple time steps are needed in order to preserve the fidelity of the load definition at the highest frequency considered. For a cyclic acoustic load, at least eight (8) time steps per cycle are used to define the peak and valley of the load definition at its highest frequency. For example, for an analysis with input frequencies up to 125 Hz, at least 1000 time steps per second are required. An acoustic time step is defined for each time step in the ANSYS solution in order to preserve the fidelity of the frequency content throughout the evaluation.

In order to address the limitations of the applied structural damping in the time domain analysis, the acoustic load definition is divided into [[ ]] portions and analyzed as separate cases. [[

]]

The available test data from instrumented steam dryers show that there is no significant pressure loading or structural response for [[

]]

When the analytical acoustic loads are first applied to the dryer at the beginning of the analysis, the structural response goes through a startup transient due to the inertia effect of the dryer (i.e. the dryer is initially assumed to be at rest). The structural response during this initial startup transient stage is not representative of steady-state operation because it is still strongly

influenced by the initial condition of the dryer. The structural response in the analysis will become independent of the initial condition of the dryer only after a large number of time steps. To minimize the initial condition effect and capture the low frequency response, the beginning of acoustic load is gradually ramped up from zero to full amplitude during the initial series of time steps. Therefore, the initial portion of the applied load time history is spent to achieve a stabilized response. A window function is applied to smooth the time history data of acoustic pressure and reduce the time needed to phase out significant initial condition effect. In the dryer analyses, direct integration solutions after half a second are generally considered sufficiently removed from the initial condition effect. [[

]] The analysis time intervals are long enough to ensure that the startup transient effects have passed.

There is an uncertainty in the predicted structural mode frequencies and dynamic response of steam dryers because of the approximations in the structural model and variations in the as-built dryer as compared to the nominal design dimensions (e.g. tolerances on plate thickness). The uncertainties in the pressure load frequency content and damping also contribute to the uncertainty in the structural analysis. Coupling of structural and acoustic modes is often a major contributor to severe stress response. Structural model uncertainty, if not addressed properly, may result in underestimating peak stress response by overlooking the actual structural modes that may be significantly excited by acoustic loads, owing to a difference between the predicted mode and the real mode.

[[

]]

Displacement boundary conditions are applied to the lug support locations in the dryer model as shown in Figure 6.1-2. The support ring rests on four to six steam dryer support brackets that are welded attachments to the RPV wall. Seismic blocks are attached to the support ring at each of the bracket locations. The motion of the steam dryer in the circumferential direction is constrained by the seismic blocks, while leaving the support free in the radial direction to

accommodate differential thermal expansion between the dryer and the RPV. Under FIV loading during normal operation, constraints in the radial direction have only a minor effect on the dryer response. Motion in the vertical direction is constrained by the dryer dead weight. For simplicity, the nodes at the locations of the support brackets are fixed in the translational degrees of freedom.

The direct integration method in the time domain was used in the FEA benchmark against the on-dryer strain measurements in Reference 3. [[

]]

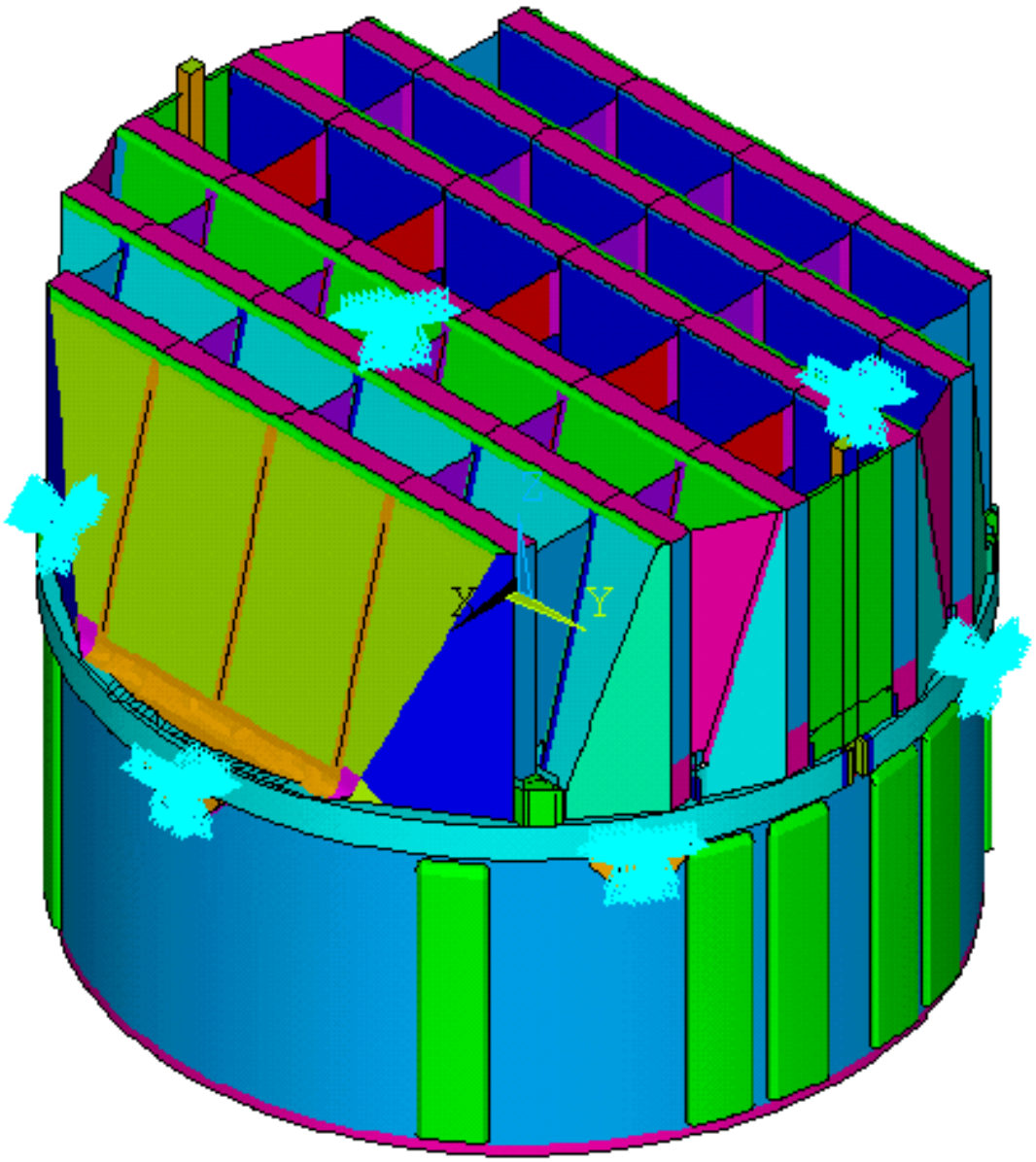

Figure 6.1-2 Steam Dryer Boundary Conditions – Dryer with Six Brackets

6.2 STRESS RECOVERY

6.2.1 Post Processing of Global FEM Analysis

The results of the dynamic stress analysis consist of time histories of the structural response of all the elements in the FEM. In the post-processing of the analysis results, the stresses of all time steps are searched in order to determine the maximum stress intensities for the dryer components. This process is called stress scoping. These maximum stress intensities are then used in the fatigue evaluation. The results for each component are scoped to obtain the maximum stress intensity directly from the analysis. In addition, the weld lines are scoped and the results adjusted by the appropriate weld factor to determine the maximum stress intensities in the weld regions. The scoping results are tabulated individually for each of the modeled steam dryer components.

Element stress intensities from ANSYS are used to represent the steam dryer stress results. Stress intensity is defined as the difference between maximum and minimum principal stresses, equivalent to twice the maximum shear stress. Element stress intensities at an element's nodal locations are extracted during the post-processing of the ANSYS results. For each shell element at a given time step, four stress intensity values are extracted from the upper layer at the four nodes associated with the element, and four more values from its bottom layer (refer to Section 5.1.1 for the definition of shell layers). The maximum of these eight values is used to represent the maximum stress intensity of this shell element at this time step. The maximum of all time steps is therefore the maximum stress intensity for this element.

In the global dryer FEM, the components of the dryer model are defined and grouped based on their common design features and relative loading. The scoping described previously for a single element is extended to all elements in a pre-defined dryer component. The maximum stress intensity is then determined for that dryer component, which is used in the fatigue evaluation. The resulting FIV stress table contains the maximum stress intensities directly from the analysis for each dryer component. An example of stress table is provided in Section 9.0. The maximum stress intensity is used in the high cycle fatigue evaluation. As described in Section 7.1, this approach is in general more conservative than using the alternating stress intensity. During the scoping process, the membrane stresses are saved for use in the ASME code-based load combination evaluations described in Section 8.0.

Stress contour plots can be generated from ANSYS based on the scoping results. They are useful in visualizing high stress regions. Figure 6.2-1 shows an example of stress contour for the inner hood panels at the time of the peak stress intensity for the panels. The plot shows that the

location of the maximum stress intensity is on the border to a hood tee. The global distribution of the relatively high stresses at this time step is also evident from the color contours.

For the high stress intensity elements located on a weld, the stress intensity value has to be modified by the appropriate weld SCF described in Section 4.2. All elements from the FEM that are either lying astride or bordering on the weld lines are identified. In addition, all nodes that are located on the weld lines are also identified. Each weld location may join together two or more different dryer components. The results are scoped for the element stress intensities for the components on both sides of the weld lines. To obtain the weld stress intensities, these stress intensities are multiplied by the appropriate weld SCF for the type of weld. The maximum weld stress intensity is then determined for each component that is associated with welds.

Each dryer component is thus identified with two values after scoping, the maximum stress intensity from the component scoping and the maximum weld stress intensity after application of the appropriate weld stress concentration factor. The larger of these two values is then used to represent the maximum stress intensity for this dryer component.

[[

]]

Figure 6.2-1 Stress Intensity Contour at Max Stress Intensity (SI) Time Step – Inner Hoods

6.2.2 Submodel Analysis and Local Stress

Submodeling is a finite element technique to obtain more accurate results in a particular region of a model. For the global dryer model, mesh convergence has been established for the general membrane and bending stresses (nominal stress). Therefore, for the high stress seen in the middle of a plate (e.g., hood panel) with no discontinuities or other stress concentration factors in its vicinity, these stresses are veritable and there is no further need for submodeling the stressed area. However, submodeling may be necessary for the high stress seen in a region of the model where stress concentration factors exist but not captured by the model. Examples include the welded connections, fillets and other geometric discontinuities. A global dryer model typically does not include these details. In summary, submodeling of steam dryers may be justified if the weld stress is significantly high in the global model, or if the high stress area is influenced by geometric discontinuities not adequately captured in the global model. Typical applications of submodeling include high-stressed welds identified by the global model results.

A submodel with much finer mesh and employing solid elements is built that includes the necessary geometric details not included in the global model. A dynamic analysis of the submodel is performed using the same time step definition from the global model. The cut boundary conditions at each time step from the global model are extracted and mapped onto the submodel. For the submodel of a weld, the analysis stress results are linearized along the weld throat to be used in the weld stress fatigue evaluation. If there is a theoretical solution applicable to the particular stress condition in a dryer region and the global model in that region is not adequate to determine the local stress, a closed form solution may be employed instead of submodeling to re-evaluate the predicted stresses from the global model in that region. To perform the closed form solution, structural forces and moments across relevant cross-sections are extracted from the global finite element model and used in the closed-form formulae from the Strength of Materials or other theoretical solutions to estimate more accurate stresses at the interested locations. An example of a closed form calculation is the stress calculation for the bank-to-bank tie bars.

For submodeling, a small area encompassing the high stress region is cut out from the global model. The size of a submodel is determined by the locations of its cut boundaries. The cut boundaries must be located sufficiently away from the high stress region so that the high gradient localized stresses will have no effect on the cut boundaries. In addition, there must be sufficient space between the cut boundaries and the high stress regions to allow adequate mesh transition. The displacement along the cut boundaries is extracted from the global model and mapped onto the same boundaries in the submodel. In order to determine whether the cut boundary conditions are applied correctly, the submodel using the original global shell mesh is first analyzed. This submodel is a portion of the global model without any modification. The same dynamic analysis

for the global model is applied to the submodel and the maximum stress results are compared to those from the global model analysis. Allowing for minimal numerical errors, the results from both models should be nearly identical.

Once the correctness of the cut boundary application is ascertained, the part of the submodel away from the cut boundaries will be refined and replaced with solid elements. Except for the area adjacent to the cut boundaries, the original mesh (typically, of shell model) is replaced with the refined solid element mesh that captures the discontinuities and other geometric details lacking in the global model. In the area adjacent to the cut boundaries, the original shell mesh is retained. In this area, the mesh is gradually transitioned to the more refined solid element mesh. Solid elements do not have the rotational DOFs that shell elements have. [[

]]

A stress convergence study is performed as described in Section 5.1.2. [[

]]

Pressure forces applied in the global model are also mapped to the submodel. After completing the submodel analysis, the submodel reaction forces at the boundaries are compared to the internal forces at the cut boundaries in the global model. This step confirms that the structural stiffness is comparable between the global model and the submodel. The force difference is found to be the smallest when the original shell mesh is retained in the vicinity of the cut boundaries in the submodel, which is the approach undertaken in meshing submodels. Figure 6.2-2 shows an example of a submodel around outlet end plates. Figure 6.2-3 shows the boundary conditions and other details of the submodel.

A full transient dynamic analysis is performed on the submodel using the same time step definition as that in the global model. This approach allows the inertia effect to be reproduced in the submodel through the time history. This is accomplished by extracting the cut boundary conditions from the global model and mapping them onto the submodel for every time step. Similar to the global model, an ANSYS load step file is generated at each time step and the transient dynamic analysis type is prescribed for the submodel.

Submodels are generally used to address the observed high stresses in the global model that are related to welds or other stress concentrations from geometry not adequately captured in the global model. [[

]]

[[

]]

Figure 6.2-2 Illustration of a Submodel Around Outlet End Plates

[[

]]

Figure 6.2-3 Boundary Conditions of a Submodel Around Outlet End Plate

[[

]]

Figure 6.2-4 Calculation of Fillet Weld Nominal Stress by Linearization

7.0 FATIGUE PREDICTION

Steam dryers are subjected to cyclic acoustic pressures that cause flow-induced vibration during normal operation. They may experience on the [[ ]] during a steam dryer's typical 40-60 year life. Therefore, HCF constitutes a major structural acceptance criterion for the steam dryer. The steam dryer fatigue evaluation described in this section is consistent with the ASME B&PV Code Section III requirements.

7.1 FATIGUE CALCULATION

In performing the fatigue evaluation for steam dryers under FIV loading, the maximum stress intensity in each dryer component is found from the FIV stress analyses described in Section 6. The maximum stress intensities are then adjusted as necessary by the appropriate weld stress concentration factors defined in Section 4.2. If the analysis is being performed in support of a plant power uprate, the adjusted stress intensities are then scaled up to the predicted EPU conditions using the EPU scaling factor described in Section 5 of Appendix A. Finally, the analysis biases and uncertainties described in Section 5.2.2 are incorporated into the results. The resulting maximum stress intensities are compared against the fatigue acceptance criterion described in Section 4.1.

The ASME Code (Section III, Div 1, NG-3222.4) prescribes the alternating stress intensity for fatigue evaluation of cyclic operations. Instead of assessing true alternating stress intensity in the dynamic cycles, the maximum stress intensity is used in the FIV fatigue evaluation of the steam dryer. The stress intensity is twice the maximum shear stress; in other words, it represents the stress range if the maximum shear stress completely reverses itself during a dynamic cycle (in this case, mean stress will be equal to zero). The alternating shear stress in the above situation is half of the stress range (or half the value of the maximum stress intensity). For the assessment of fatigue acceptance, the full value of maximum stress intensity is compared against the fatigue limit. The maximum stress intensity is in general a more conservative approach than alternating stress intensity in such fatigue evaluation.

The requirement for acceptance of a dryer component is that its maximum stress intensity has to be smaller than the fatigue limit. [[

]]

[[

]]

Figure 7.1-1 Primary and Weld Scoping for Fatigue Evaluation

7.2 FREQUENCY CONTENT OF THE STRUCTURAL RESPONSE

The frequency content of the stresses is analyzed for the components with small safety factors as identified by the fatigue evaluation. The frequency content of strain and peak stress over multiple frequency bands is factored into the calculation of the overall stress bias in the RMS method described in Section 5.2.2.

8.0 ASME LOAD COMBINATIONS

The steam dryer is not a safety component and performs no active safety function. However, the dryer must maintain its structural integrity (i.e. generate no loose parts) so as to not interfere with the function of a safety system. The following section discusses the methodology used for the primary stress assessment of the steam dryer and the RPV support brackets. The results of this assessment demonstrate that the dryer will maintain its structural integrity during transient and accident events. Guidance is provided by Article NG-3000 of Reference 1 for the steam dryer and Article NB-3000 of Reference 1 for the attachments to the RPV shell.

8.1 ASME LOAD COMBINATIONS

Load combinations are defined for the evaluation of the primary stresses in the steam dryer for Normal (Service Level A), Upset (Service Level B), Emergency (Service Level C), and Faulted (Service Level D) conditions. The load combinations are specified in the Steam Dryer Design Specification and associated data sheet. Table 8.1-1 provides a typical set of load combinations applied to the steam dryer. Plant-specific design basis load combinations will be used.

Table 8.1-1 ASME Load Combinations and Conditions

Comb. no	Level	Combination
A-1	Normal	[[
B-1	Upset	
B-2	Upset	
B-3	Upset	
B-4	Upset	
B-5	Upset	
C-1	Emergency	
D-1	Faulted	
D-2	Faulted	
D-3	Faulted	
D-4	Faulted	
D-5	Faulted	]]

Notes:

1. Loads from independent dynamic events are combined by the square root sum of the squares method.
2. The load combination table is typical. Plant-specific design basis load combinations will be used.

Definition of Load Acronyms

[[

]]

8.2 ASME APPROACH

The global FE shell model described in Section 5.1 is used in these analyses. The structural responses of the steam dryer to the ASME load combinations will be evaluated using the ANSYS finite element code for the loads defined in Section 8.1. The results of the individual load analyses are then combined for each event as specified in Table 8.1-1. The type of finite element structural analysis for each load term in Table 8.1-1 is identified in Table 8.2-1. [[

]].

Table 8.2-1 Type of Analysis for the Load Terms in ASME Load Combinations

Load Term	Description	Type of Analysis for the Load
[[		
		]]

Note:

DLF Dynamic Load Factor: The static analysis stress results are multiplied by this factor to adjust for the effect from transient events.

8.3 ASME LOAD CASE STRESS RESULTS

The stress intensity representing the FIV membrane stress is obtained from the FIV analysis for every component and every load. The results of the individual load analyses are then combined for each event as specified in Table 8.1-1. The resulting stresses are then compared to the criteria from Section 4.1. Table 9.0-4 in Section 9 provides a template table for reporting the maximum stress intensity values of dryer components. Minimum stress margins are also calculated in the table.

8.4 ASME CODE ANALYSIS OF THE RPV DRYER BRACKETS

The following section covers the steam dryer components that support the dryer within the RPV. These components are the steam dryer support brackets and the guide rod brackets. While the steam dryer analyses take guidance from Article NG-3000 of Section III of the ASME BPV Code (Reference 1), the brackets attached to the RPV are governed by Article NB-3000 and Appendix F of the same Code. Also, note that the analyses of these brackets falls into the "Safety Related" category because these brackets are attached to the reactor vessel pressure boundary.

The guide rod bracket provides a load path to the RPV only during dryer installation; therefore, the following paragraphs will primarily focus on the support brackets (lugs) and the RPV near the lugs.

Table 9.0-5 shows a typical minimum margin stress summary table. This table will be referred to throughout the following paragraphs.

8.4.1 Load Cases

The load combinations to be considered are defined by the design basis for the plant and the RPV. The certified design specification for the steam dryer brackets provides guidance with regard to the load combinations and load types that are to be considered. The load combinations considered are similar to those in Table 8.1-1 and additional design and installation load combinations are analyzed per the steam dryer bracket design specification.

8.4.2 Primary Stress

The primary stress intensity values required by the code are general primary membrane (Pm), local primary membrane (PL) and membrane plus bending (PL + PB). Special stress categories such as the maximum shear stress and bearing stress are also calculated as part of the primary stress assessment.

The primary stress values in the RPV shell and the steam dryer brackets are determined differently. [[

]]

8.4.2.1 RPV Primary Stress Assessment

The primary membrane stress intensity due to the design pressure is determined using closed form equations. This stress intensity value is compared to Sm (see Table 9.0-5).

[[

]]

[[

]]

Figure 8.4-1 Typical Steam Dryer Bracket FEM

The forces experienced by the bracket for the load combinations for the various service levels are applied to the contact area between the bracket and the steam dryer and run using static analysis. The model is then post processed to determine the following stress intensity values for each load combination:

1. [[

2.

]]

8.4.2.2 Dryer Bracket Primary Stress Calculations

[[

]]

[[

]]

Figure 8.4-2 Bracket Stress Calculation Locations

[[ ]] The calculations include the evaluation of primary membrane stress intensity, primary membrane plus bending stress intensity, and the primary and maximum shear stress in the bracket. [[

]]

The code allowable values for the general and local primary membrane, local membrane plus bending, and the average and maximum shear stress values are provided in Table 9.0-5. Note that the upset condition (Service Level B) allowable values are increased by 10% over the normal operating condition values per Code (Reference 1). The faulted (Service Level D) condition allowable stress values are governed by Appendix F of Reference 1.

8.4.3 Secondary Stress Range

For the normal and upset plant conditions, the code requires a check of the local primary membrane (PL) plus primary bending (PB) plus the secondary stress range (Q) at this location. The PL + PB + Q stress is compared to 3.0Sm.

8.4.3.1 RPV Shell

For the RPV shell in the evaluation of the primary plus secondary stress range (PL + PB + Q) for the normal and upset conditions, the pressure stress in the RPV shell dominates. Therefore, the maximum primary local membrane plus bending (PL + PB) is increased by the secondary stress range (Q) from the thermal cycling due to the start up and shut down transients. This stress range is usually obtained from the original stress report for the RPV. This report has the thermal stress due to the startup and shutdown transients at various locations of the RPV shell. [[

]]

8.4.3.2 Steam Dryer Bracket

Because the materials used for the support bracket are usually similar with respect to thermal expansion coefficients, the only loading that produces a secondary stress in the dryer bracket at the bracket-to-RPV interface is due to internal pressure cycling. [[

]]

8.4.4 Analysis for Cyclic Operation

An assessment is performed to determine the suitability of the bracket and shell at the bracket location to the vibratory environment. This assessment is governed by paragraph NB-3222.4 (d) of the Code (Reference 1). This paragraph is entitled "Components Not Requiring Analysis for Cyclic Operation," and sets forth the criterion for fatigue analysis exemption (i.e. no cycle counting required). This is also known as a fatigue exemption assessment.

Parts NB-3222.4 (d)(1) - (5) discuss the requirements on the usage with regard to the atmospheric to service pressure cycles, normal service pressure fluctuations, and temperature differences. The Reactor Pressure Vessel Stress Report for the particular plant in operation typically provides evidence that these criteria are met for the RPV shell and its attachments.

Part NB-3222.4 (d)(6) discusses mechanical loads. The locations evaluated for the mechanical fatigue assessment are the same as those for the bracket primary stress analysis in Section 8.4.2.2. This approach is appropriate for the evaluating the bracket fatigue with regard to mechanical loading where the resulting stress range is then compared with the allowable stress amplitude. Here the code is assigning a stress concentration value of two, with the total cumulative number of significant cycles used for the fatigue exemption determination of a load condition.

In the mechanical load fatigue exemption, the specified full range of mechanical loads excluding pressure must not result in load stresses whose range exceeds the alternating stress allowable (Sa) value from the applicable fatigue curve for the total specified number of significant load fluctuations. [[

]]

[[

]] This value is compared with the Sa allowable for the total design cycles for significant loads.

[[

]]

9.0 PLANT SPECIFIC REPORT CONTENT

The plant-specific steam dryer stress report includes information on the finite element model, material properties, analysis methodology, FIV load definition, design basis load combinations, and structural acceptance criteria used in the analysis. It presents the results of the fatigue analysis and the primary stress analysis. Plant-unique special analyses and supporting justifications are also provided in the plant-specific steam dryer stress report.

This subsection provides templates for tabulated final stress processing that are common to all dryer analyses. Typical dryer components are listed. Tables 9.0-1 and 9.0-2 document the process of determining the maximum stress intensity of each dryer component for the [[ ]] analyses, respectively. The maximum stress intensities from both the primary scoping and the weld scoping are tabulated for the nominal run and all time shift runs so that both weld stress and structural uncertainty are included in the maximum component stresses. Table 9.0-3 documents the process of determining the final stress intensities. It includes combining the [[ ]] stresses, scaling to EPU and adjusting for the analysis bias and uncertainty. For the example shown in Table 9.0-3, a single bias and uncertainty factor is applied to both [[ ]] results. If the bias and uncertainty is different for the [[ ]] stress intensities will be scaled to EPU and adjusted for the bias and uncertainty separately prior to final combination. Table 9.0-3 also documents the final safety factor calculation.

In addition to the stress tables described above, Table 5 of Enclosure 2, Attachment 1 in Reference 3, and Tables 4 and 5 of Enclosure 2, Attachment 2 in Reference 3 provide the templates for overall bias and uncertainty evaluation once the individual bias and uncertainty terms are obtained. The first demonstrates an example of calculating total PBLE and FE stress bias and uncertainty as well as the associated bias and uncertainty. The second demonstrates an example of calculating regional PBLE stress bias and the associated load factor. The third demonstrates how to apply the regional PBLE stress bias to a dryer.

The primary stress analysis results table templates are shown in Tables 9.0-4 and 9.0-5.

Table 9.0-1 Maximum Stress Intensities after Scoping – [[ ]] (Template)

COMPONENT	[[ ]] - Maximum Stress Intensity (psi)																		Applied Weld Factor for weld scoping	LF Max Stress Intensity (psi)	Load Case at Max Stress
	NOM		P10		P75		P5		P25		M25		M5		M75		M10				
	Primary scoping	Weld scoping	Primary scoping	Weld scoping	Primary scoping	Weld scoping	Primary scoping	Weld scoping	Primary scoping	Weld scoping	Primary scoping	Weld scoping	Primary scoping	Weld scoping	Primary scoping	Weld scoping	Primary scoping	Weld scoping			
Dryer Base Plate																					
Trough Thin Section																					
Trough Thick Section																					
Bank Top Cap - Inner																					
Bank Top Cap - Outer																					
Bank End Plates - Inner																					
Bank End Plates - Outer																					
Outlet End Plates - Inner																					
Outlet End Plates - Outer																					
Hoods - Inner																					
Hoods - Outer																					
Divider Plates																					
Inlet End Plates - Inner																					
Inlet End Plates - Outer																					
Skirt																					
Drain Pipes																					
Drain Channels																					
Lower Skirt Ring																					
Cover Plates																					
Hood Tees - Inner																					
Hood Tees - Outer																					
Support Ring																					
Tie Bars Bank-to-Bank																					
Hood Supports																					

Table 9.0-2 Maximum Stress Intensities after Scoping – [[ ]] (Template)

COMPONENT	[[ ]] - Maximum Stress Intensity (psi)																		Applied Weld Factor for weld scoping	HF Max Stress Intensity (psi)	Load Case at Max Stress
	NOM		P10		P75		P5		P25		M25		M5		M75		M10				
	Primary scoping	Weld scoping	Primary scoping	Weld scoping	Primary scoping	Weld scoping	Primary scoping	Weld scoping	Primary scoping	Weld scoping	Primary scoping	Weld scoping	Primary scoping	Weld scoping	Primary scoping	Weld scoping	Primary scoping	Weld scoping			
Dryer Base Plate																					
Trough Thin Section																					
Trough Thick Section																					
Bank Top Cap - Inner																					
Bank Top Cap - Outer																					
Bank End Plates - Inner																					
Bank End Plates - Outer																					
Outlet End Plates - Inner																					
Outlet End Plates - Outer																					
Hoods - Inner																					
Hoods - Outer																					
Divider Plates																					
Inlet End Plates - Inner																					
Inlet End Plates - Outer																					
Skirt																					
Drain Pipes																					
Drain Channels																					
Lower Skirt Ring																					
Cover Plates																					
Hood Tees - Inner																					
Hood Tees - Outer																					
Support Ring																					
Tie Bars Bank-to-Bank																					
Hood Supports																					

Table 9.0-3 Maximum Stress Intensity and MASR from FIV Analysis (Template)

DRYER COMPONENT	CLTP MAXIMUM STRESS INTENSITY (PSI)	EPU MAXIMUM STRESS INTENSITY (PSI)					MAX STRESS INTENSITY (PSI)	MASR
		SRV Freq #1	SRV Freq #2	SRV Freq #3	SRV Freq #4	SRV Freq #5		
Dryer Base Plate								
Trough Thin Section								
Trough Thick Section								
Bank Top Cap - Inner								
Bank Top Cap - Outer								
Bank End Plates - Inner								
Bank End Plates - Outer								
Outlet End Plates - Inner								
Outlet End Plates - Outer								
Hoods - Inner								
Hoods - Outer								
Divider Plate								
Inlet End Plates - Inner								
Inlet End Plates - Outer								
Skirt								
Drain Pipes								
Drain Channel								
Lower Skirt Ring								
Cover Plate								
Hood Tee - Inner								
Hood Tee - Outer								
Support Ring								
Tie Bars Bank-to-Bank								
Tie Bars at center								
Trans Brace under Base Plate								
Trans Brace Brackets								
Hood Support								
Holddown								

Table 9.0-4 Typical ASME Stress Table for the Steam Dryer (Template)

Component	Normal		Upset						Emergency		Faulted							
	A1		B1		B2		B3		C1		D1		D2		D3		D4	
	Pm	Pm+b	Pm	Pm+b	Pm	Pm+b	Pm	Pm+b	Pm	Pm+b	Pm	Pm+b	Pm	Pm+b	Pm	Pm+b	Pm	Pm+b
Dryer Base Plate																		
Trough Thin Section																		
Trough Thick Section																		
Bank Top Cap – Inner																		
Bank Top Cap – Outer																		
Bank End Plates – Inner																		
Bank End Plates – Outer																		
Outlet End Plates – Inner																		
Outlet End Plates – Outer																		
Hoods – Inner																		
Hoods – Outer																		
Inlet End Plates – Inner																		
Inlet End Plates																		
Skirt																		
Drain Plugs																		
Lower Skirt Ring																		
Cover Plate																		
Hood Tee – Inner																		
Hood Tee – Oouter																		
Support Ring																		
Tie Bars Bank-to-Bank																		
Tie Bars at center																		
Trans Brace under Base Plate																		
Trans Brace Brackets																		
Bank Top Cap – Inner (no TieBar)																		
Bank Top Cap – Outer (no TieBar)																		
Divider Plate – Inner Banks																		
Divider Plate – Outer Banks																		
Hood Support – Inner Banks																		
Hood Support – Outer Banks																		
Drain Channel – radial leg																		
Drain Channel – circum portion																		
Bank Top Cap – Inner																		
Bank Top Cap – Outer																		
304L SS Allowable Stress	14350	21525	15785	23678	15785	23678	15785	23678	21525	32288	34440	51660	34440	51660	34440	51660	34440	51660
Max Stress / Allowable																		

Table 9.0-5 Table of Minimum Design and Operational Stress Margins (Template)

Service Condition	Component	Stress Category	Requirement	Allowable Value [psi]	Maximum Predicted Value [psi]	Stress Margin	Remarks
DESIGN	Dryer Bracket	P_m	$1.0S_m$				
	Vessel Shell		$1.0S_m$				
	Dryer Bracket	Maximum Shear	$0.8S_m$				
	Vessel Shell		$0.8S_m$				
	Dryer Bracket	$P_L + P_B$	$1.5S_m$				
	Vessel Shell		$1.5S_m$				
	Dryer Bracket	Bearing Stress	$1.0S_y$				
	Vessel Shell		N/A	N/A	N/A	N/A	
NORMAL	Dryer Bracket	P_m	$1.0S_m$				
	Vessel Shell	P_L	$1.5S_m$				
	Dryer Bracket	$P_L + P_B$	$1.5S_m$				
	Vessel Shell		$1.5S_m$				
	Dryer Bracket	Maximum Shear	$0.8S_m$				
	Vessel Shell		$0.8S_m$				
	Dryer Bracket	$P_L + P_B + Q$	$3.0S_m$				
	Vessel Shell		$3.0S_m$				
	Dryer Bracket	Bearing Stress	$1.0S_y$				
	Vessel Shell		N/A	N/A	N/A	N/A	
	Dryer Bracket	FATIGUE	Exemption from Fatigue Analysis per NB-3222.4 see Section X.XX				
	Vessel Shell						
UPSET	Dryer Bracket	P_m	$1.1S_m$				
	Vessel Shell	P_L	$1.65S_m$				
	Dryer Bracket	$P_L + P_B$	$1.65S_m$				
	Vessel Shell		$1.65S_m$				
	Dryer Bracket	Maximum Shear	$0.88S_m$				
	Vessel Shell		$0.88S_m$				
	Dryer Bracket	$P_L + P_B + Q$	$3.3S_m$				
	Vessel Shell		$3.3S_m$				
	Dryer Bracket	Bearing Stress	$1.0S_y$				
	Vessel Shell		N/A	N/A			
	Dryer Bracket	FATIGUE	Exemption from Fatigue Analysis per NB-3222.4 see Section X.XX				
	Vessel Shell						
FAULTED	Dryer Bracket	P_m	$Min(0.7S_u$ or $2.4\ S_m)$				
	Vessel Shell		$Min(0.7S_u$ or $2.4\ S_m)$				
	Dryer Bracket	P_L	$1.5*(Min(0.7S_u$ or $2.4\ S_m))$				
	Vessel Shell		$1.5*(Min(0.7S_u$ or $2.4\ S_m))$				
	Dryer Bracket	$P_L + P_B$	$1.5*(Min(0.7S_u$ or $2.4\ S_m))$				
	Vessel Shell		$1.5*(Min(0.7S_u$ or $2.4\ S_m))$				
	Dryer Bracket	Primary Shear	$0.42S_u$				
	Vessel Shell		$0.42S_u$				
	Dryer Bracket	Maximum Shear	$0.9S_u$				
	Vessel Shell		$0.9S_u$				

Table Notes

10.0 CONCLUSIONS

This report defines the methodology for the structural analysis of steam dryers in response to FIV loads. The report describes the detailed finite element model, analysis procedures, fatigue evaluation and ASME load combinations of steam dryers used in the BWR/2 through BWR/6 and ABWR product line. The FIV loads defined in Appendices B and C are applied in the structural analysis. The structural analysis results will be used to iterate on steam dryer designs that will meet the required fatigue and ASME load combination stress criteria.

11.0 REFERENCES

1. American Society of Mechanical Engineers Boiler and Pressure Vessel Code (ASME B&PV), Section III, 2001 Edition.

2. ANSYS® Release 11.0SP1, Ansys Incorporated, 2007.

3. GEH Letter MFN 09-509 from Richard E. Kingston (GEH) to USNRC Document Control Desk, "Response to Portion of NRC RAI Letter No. 220 and 339 Related to ESBWR Design Certification Application – DCD Tier 2 Section 3.9 – Mechanical Systems and Components; RAI Numbers 3.9-213 and 3.9-217 S01." Dated July 31, 2009, Docket Number 52-010.

4. Letter, Entergy to USNRC, "Vermont Yankee Nuclear Power Station Report on the Results of Steam Dryer Monitoring," BVY 06-056 (Docket No. 50-271, TAC No. MC0761), Dated June 30, 2006.

5. 0000-0101-0766-P-R0, "Main Steam Line Limit Curve Adjustment during Power Ascension," Class III, April 2009.

Appendix F

Power Ascension Test Plan

TABLE OF CONTENTS

LIST OF TABLES

LIST OF FIGURES

F.1 Background

The GGNS replacement dryer was analyzed for CLTP loads projected to EPU based on [[ ]]. This projected load was combined with [[ ]].

The following cases describe the [[ ]] conditions considered in the design basis stress analysis:

[[

]]

During the testing performed up to CLTP (Appendix G), acoustic signals in the MSL strain gauge data [[

]]

[[

]]

Following the methodology outlined in Appendix A, design basis stress analyses were performed using the GGNS plant specific MSL strain gauge data obtained over a range of power. The design basis stress analysis accounted for the expected increase in loads as steam velocity increases, including the effect of potential SRV resonances. The stress analysis results included the analysis and measurement biases and uncertainties. The design basis peak stress represents the maximum calculated stress in any dryer component.

The limit curve approach used for dryer power ascension monitoring was first used by Entergy at Vermont Yankee in monitoring the modified steam dryer during power ascension testing in 2006. The limit curve approach was later adopted by GEH in the development of main steam line monitoring limits for the prototype BWR/4 Units 1 and 2 replacement steam dryers (Reference 1). During the power ascension at Vermont Yankee, [[

]] (Reference 2). [[

]] development of the prototype BWR/4 Limit Curve adjustment methodology (Reference 3). This methodology was employed for MSL monitoring and the adjustment of acceptance limits during power ascension testing of the prototype BWR/4 Units 1 and 2 steam dryers. This general methodology has been incorporated into the GGNS acceptance limits presented here. For the GGNS Power Ascension Test Program (PATP), [[

]] will be based on the MSL strain gauge measurements obtained during the power ascension following the same methodology [[

]].

F.2 Methodology for Development of Acceptance Limits

During power ascension testing above CLTP, the MSL strain gauge data will be used [[

]]

[[

]]

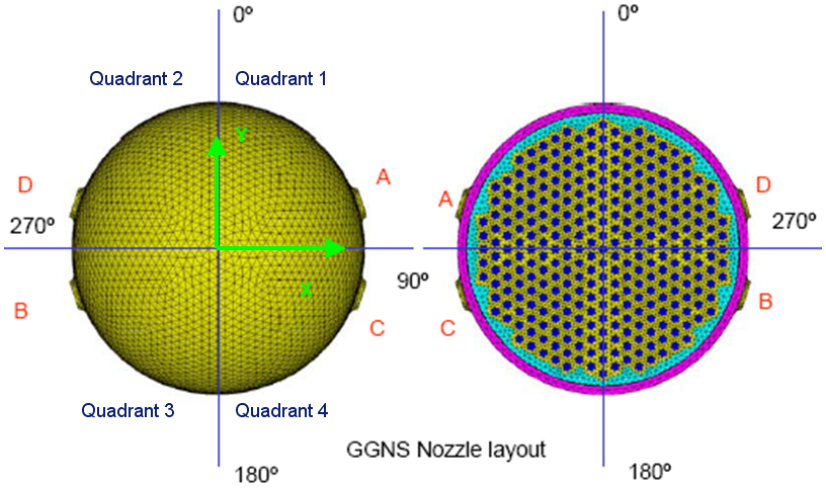

Figure F-1. GGNS MSL Layout

[[

]]

Figure F-2. [[ ]]

[[ ]]

[[

]]

Figure F-3. [[ ]]
[[ ]]

[[

]]

Figure F-4. [[ ]]
[[ ]]

[[

]] Maintaining these [[ ]] acceptance limits will assure the dryer peak stress amplitude remains below 13,600 psi, the ASME Curve C endurance limit for the dryer material. Previous steam dryer monitoring programs at the prototype BWR/4 plant (Reference 1) and Vermont Yankee (Reference 2) had developed monitoring limits based on MSL strain gauge PSD data. [[

]]

The dryer stress response was evaluated [[

]]. The structural model was evaluated for frequency variations over a ±10% range by varying the time step size for the load definition. [[

]]

[[

]]

Figure F-5. [[ ]]

[[

]]

Figure F-6. [[ ]]

The projected limiting stress at [[
]] in Table F-1. [[

]]

Table F-1. Design Basis Peak Stress Intensities

Condition	Limiting Subcomponent	Peak Stress (psi)	[[
			]]

[[ ]]

The Level 1 limit curve is established by factoring the EPU design load spectra by the Limit Curve Factor (LCF). [[

]]

The Level 1 limit is depicted as the upper red curve [[
]]. If a Level 1 limit is exceeded, power will be reduced to a level where the limit curve is satisfied. The goal during the PATP is to maintain the [[ ]] below the Level 2 limit.

During power ascension to EPU power levels, [[

]]

[[

]]

Maintaining the [[ ]] below the acceptance limits will assure that the FIV peak stress amplitude on the GGNS replacement dryer will remain below the ASME Code endurance limit.

F.3 GGNS Dryer Acceptance Limits for Operation Above CLTP

The limits provided in this section shall be evaluated at power ascension plateaus not to exceed 3.5% core thermal power intervals while the reactor steam flow and core thermal power are essentially constant. If a Level 1 limit is exceeded, power will be reduced to a level where the limit criteria are satisfied. The goal during the PAT is to maintain the [[ ]] below the Level 2 limit.

[[ ]] monitored and trended. The trends should be used to extrapolate the dryer loads to the next power ascension plateau. [[

]]

During initial power ascension above CLTP the following acceptance limits shall be maintained:

[[

]]

[[

]]

During the first complete cycle of operation with the replacement steam dryer, monitoring of plant parameters potentially indicative of steam dryer structural degradation will be conducted as recommended in Service Information Letter (SIL) 644, Revision 2 (Reference 4). During the refueling outage following the first complete cycle of operation with the replacement steam dryer, inspections of the dryer will be conducted as recommended in Reference 4.

[[

]]

Figure F-7. [[ ]]

[[

]]

Figure F-8. [[ ]]

[[

]]

Figure F-9. [[ ]]

[[

]]

Figure F-10. [[ ]]

[[

]]

Figure F-11. [[ ]]

[[

]]

Figure F-12. [[ ]]

[[

]]

Figure F-13. [[ ]]

[[

]]

Figure F-14. [[ ]]

[[

]]

Figure F-15. [[ ]]

[[

]]

Figure F-16. [[ ]]

[[

]]

Figure F-17. [[ ]]

[[

]]

Figure F-18. [[ ]]

Table F-2. [[ ]]

[[				
				]]

Table F-3. [[ ]]

[[				
				]]

Table F-4. [[

]]

[[				
				]]

Table F-5. [[

]]

[[				
				]]

Table F-6. [[

]]

[[				

]]

Table F-7. [[

]]

[[				
				]]

F.4 Requirements for Defining [[ ]]

[[

]]

[[

]]

F.5 Determine Margin for Continued Power Ascension

At each power ascension plateau, the data trending described in Section 5 of Appendix A [[

]]

F.6 Update Acceptance Limits

F.6.1 Prepare [[ ]]

Based on trending data and [[

]]

[[

]]

F.6.2 Determine Adjusted Stress with Bias and Uncertainty

With revised EPU [[

]]

F.6.3 Updated Acceptance Limits

Using revised [[

]]

F.7 References

1. GE Hitachi Nuclear Energy, "Revised Susquehanna Replacement Steam Dryer Limit Curves – Main Steam Line Mounted Instrumentation," 0000-0096-5766-P-R1, February 2009.

2. Letter, Entergy to USNRC, "Vermont Yankee Nuclear Power Station Report on the Results of Steam Dryer Monitoring," BVY 06-056 (Docket No. 50-271, TAC No. MC0761), dated June 30, 2006.

3. GE Hitachi Nuclear Energy, "Main Steam Line Limit Curve Adjustment During Power Ascension," 0000-0101-0766-P-R0, April 2009.

4. General Electric Service Information Letter SIL No. 644 Rev. 2, "BWR Steam Dryer Integrity," August 30, 2006.

Appendix G

Grand Gulf Nuclear Station Main Steam Line Test Report

TABLE OF CONTENTS

LIST OF TABLES

LIST OF FIGURES

1.0 Summary

During RFO-16 strain gauges were installed on all four main steam lines at the Grand Gulf Nuclear Station (GGNS). The data from these gauges provides input to the GEH Plant Based Load Evaluation (PBLE), which will be used to determine pressure loads on the steam dryer at Current Licensed Thermal Power (CLTP) and to predict the pressure loads at Extended Power Uprate (EPU) condition. As part of the detailed EPU analysis these loads will be utilized in conjunction with Finite Element Analysis to evaluate the dryer's structural capabilities at EPU. This report provides a preliminary evaluation of the quality of the data and the frequencies of concern.

[[ ]] strain gauges were placed in [[ ]] locations ([[ ]] locations on Main Steam Line (MSL) B and D, as well as [[ ]] locations on MSL A and C) determined by acoustic finite element modeling of the steam lines and vessel. Additional surface preparation of the MSL piping was required due to significant scale buildup. Of the [[ ]] strain gauges, [[ ]] remained functional after installation/final testing. When analyzed the signals showed very low noise and good signal quality.

Power Spectral Density (PSD) analysis of the MSL data showed notable maxima at 12 Hz, 23 Hz and 44 Hz. All of these maxima are indicative of acoustic modes in the combined steam dome and MSL system excited by flow through the upstream and downstream MSIVs and MSL venturis. SRV resonances were observed at 196 Hz, 203 Hz and possibly 208 Hz in the 100% CLTP measurements.

2.0 Purpose

The purpose of this report is to provide the results of the data acquisition and initial analysis from the MSL pressure measurements at the GGNS. Strain gauges mounted on the surface of the MSLs within the drywell were used to measure the dynamic pressure waves during power ascension and steady state operation. This data is used as input to the PBLE to define the fluctuating pressure loads for the structural analysis of the steam dryer. More detailed evaluation of this data is contained in Section 3 of the main report.

3.0 Instrumentation

3.1 Strain Gauges

The MSL sensors consisted of [[ ]] high temperature weldable strain gauges with 3-wire shielded leads (HITEC part number HBWAK-35-250-6-10FG Shield). The selection of the sensors was based on past experience of similar tests conducted on other plant MSLs. The strain gauge arrangement consisted of [[ ]] monitoring locations (upper and lower) on MSLs B and D, as well as [[ ]] monitoring locations on MSLs A and C. [[ ]] strain gauges were oriented circumferentially at each monitoring location with the strain gauge pairs on

opposite sides (i.e., 180° apart) wired in series. The strain gauges were wired in series, because there were a limited number of penetration cables available.

3.2 Sensor Installation

Strain gauge installation began on September 24, 2008 and was completed on October 11, 2008. The strain gauges were installed at the primary elevations on the MSL piping inside the primary containment. A capacitive discharge welder was used to install the strain gauges onto the MSLs. Figure 1 illustrates the primary strain gauge elevations. Field measurements of the strain gauge locations are referenced to the MSL nozzle elevation centerline (Table 1). This reference is assumed to be at [[ ]]. The installation dimensions are the vertical measurement relative to the vessel nozzle. The purpose of these as-built dimensions is to derive the adjusted distance from the inside of the vessel to gauge locations along the center of the steam line. In the acoustic model the pipe is represented as a one-dimensional component based on the pipe centerline. The linear distance dimensions used in the GEH location assessment were based on plant drawings provided by Enercon. These drawings provided as-built dimensions that permitted GEH to determine the distance from the inside wall of the vessel to riser. Linear distances from the vessel nozzle to the actual strain gauge locations were calculated from the plant drawings and the as-built dimensions, measured within 1/8”, and are shown in Table 2.

Table 1. GGNS Plant As-Built Measurements

[[

]]

Table 2. Linear Distance from Vessel Nozzle to Strain Gauge Locations

Strain Gauge Locations	Distance to Inside Nozzle, inches			
	MSL B	MSL D	MSL A	MSL C
[[				
				]]

The strain gauge installation required the removal and reinstallation of the MSL insulation at the specified strain gauge locations. The insulation was modified to accommodate space for the strain gauges on the MSL pipes and for the signal cable egress. Post installation testing identified several failed strain gauges. All were repaired and of the [[ ]] strain gauges, [[ ]] remained operational throughout the test. A sample of installed strain gauge photos can be found in Figures 2 through 8.

[[

]]

Figure 1. Primary Strain Gauge Attachment Elevations

[[

]]

Figure 2. Photo Strain Gauge MSL A 3rd

[[

]]

Figure 3. Photo Strain Gauge MSL B Upper

[[

]]

Figure 4. Photo Strain Gauge MSL B Lower

[[

]]

Figure 5. Photo Strain Gauge MSL C Upper

[[

]]

Figure 6. Photo Strain Gauge MSL C Lower

[[

]]

Figure 7. Photo Strain Gauge MSL D Upper

[[

]]

Figure 8. Photo Strain Gauge MSL D Lower

3.3 Data Acquisition System

The DAS was located on a cart inside the auxiliary building at elevation 139'. It consisted of the LMS SCADAS Mobile unit, 700-Ohm resistor bridge completion box, data acquisition laptop computer and analysis laptop computer. Signal conditioning for the strain gauges was contained in the LMS SCADAS modules. An isolation transformer was placed between the DAS and the plant AC power to eliminate electrical noise. A photo of the DAS setup inside the auxiliary building can be seen in Figure 9.

The DAS wiring diagram is shown in Figure 10 and only illustrates one shielded twisted pair of a cable. All sensor leads from the strain gauges were first wired in series. Field cabling connected the strain gauge pairs to the inboard junction box for penetration TB1CE01. These cables were connected to existing terminations. Additional field cabling connected the outside junction box at penetration TB1CE01 to the external 700-Ohm resistor bridge completion box. The bridge completion box interfaced with the DAS (LMS SCADAS Mobile Unit and interfacing laptop computer) via short cables.

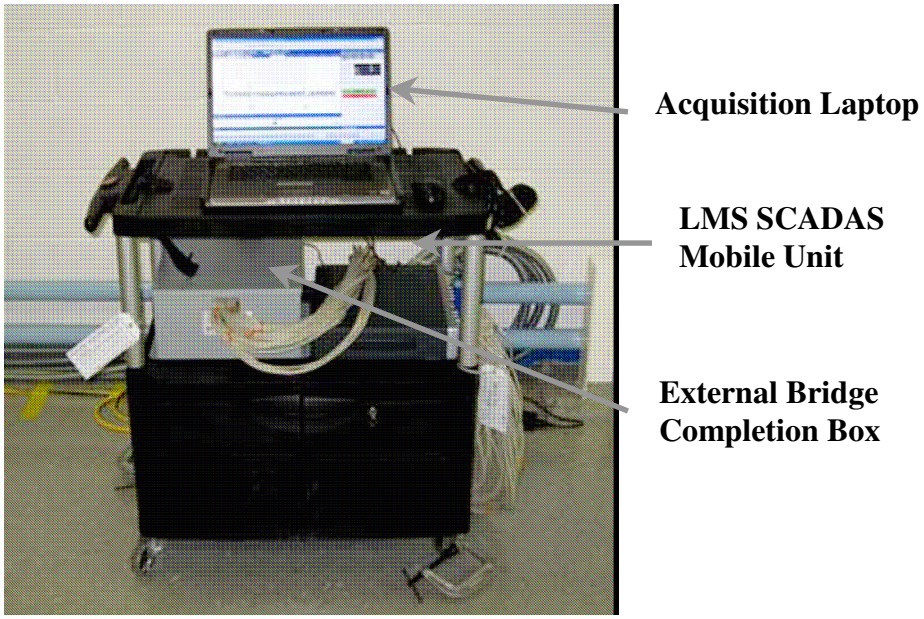

Figure 9. DAS Photo Inside Auxiliary Building

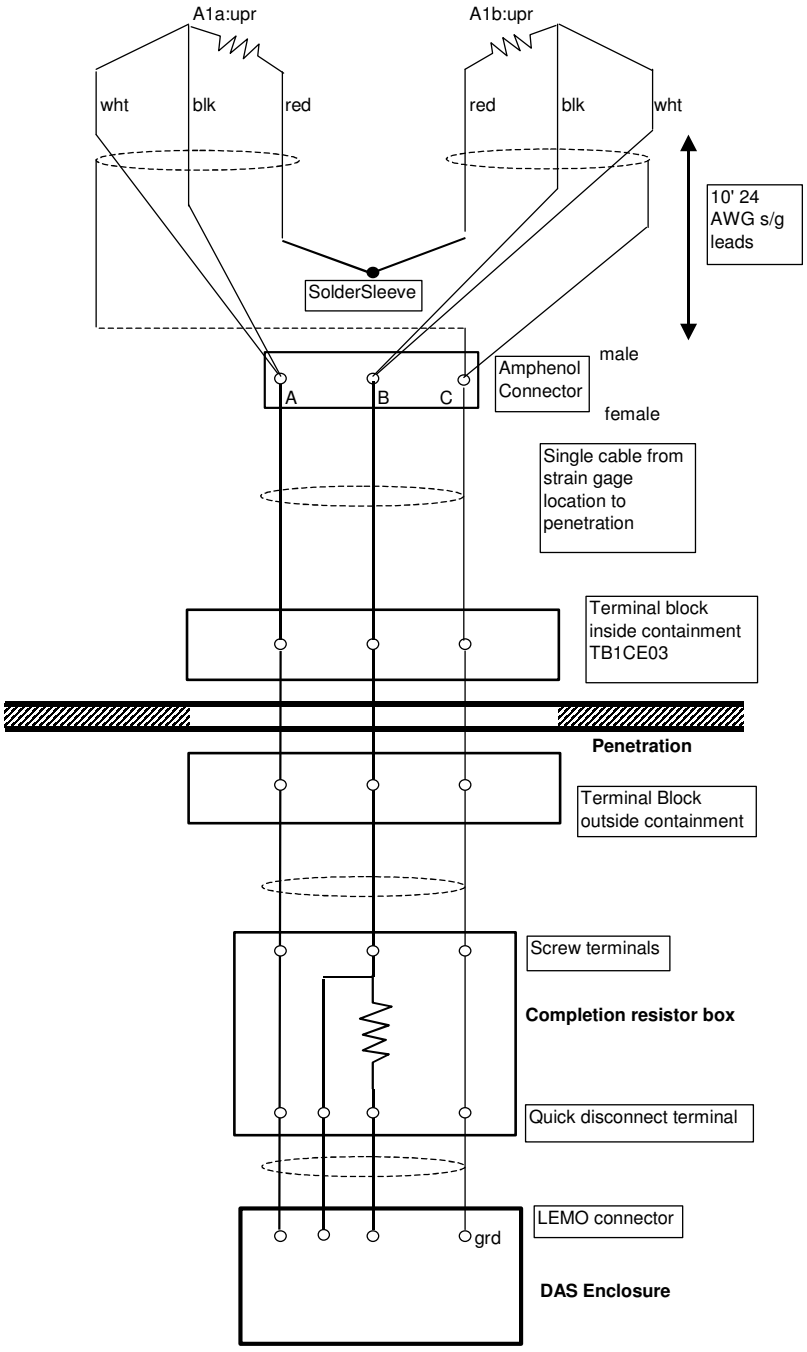

Figure 10. DAS Wiring Diagram

4.0 Tests Performed

4.1 Sensor Pre-Calibration

The sensors were pre-calibrated on October 8, 2008 at the GGNS through the LMS Data Acquisition System (DAS). No abnormalities were noted.

4.2 Primary System Pressurization Test

After the sensor pre-calibration the strain gauges were measured statically during the Primary System Pressurization Test on October 16-17, 2008. Transient records during pressurization and de-pressurization conditions were recorded. The static strain levels were then converted to equivalent pressure using the MSL dimensions and compared with plant pressure instrumentation.

4.3 Power Ascension

Steady state power conditions were used to measure the fluctuating pressure in the MSLs. Measurements were taken at approximately [[
]]. Power ascension data was taken from November 1, 2008 to November 3, 2008. After the reactor stabilized, [[ ]] additional 100% CLTP data points were collected at approximate one hour intervals on November 4, 2008.

4.4 Sensor Post-Calibration

The sensors were post-calibrated on November 5, 2008 with the LMS DAS. No abnormalities were noted.

4.5 Low Power Measurements

During RFO-17 in May 2010, these strain gauges were used to measure static and dynamic signals to evaluate the noise floor level and electrical and mechanical noise at low power levels. Steady state power conditions were used to measure the fluctuating pressure in the MSLs. Measurements were taken at [[
]]. Power ascension data was taken from May 26, 2010 to May 27, 2010. The low power measurements are summarized in Attachment D.

5.0 Data Acquisition Analysis

5.1 Data Acquisition and Analysis Process

The MSL vibration data was collected with a laptop computer and a LMS SCADAS Mobile unit using a sampling frequency of [[ ]]. The only exception was the third data set of the [[ ]] CLTP steady state point. The sampling rate was increased to [[ ]] to check

for aliasing, but no aliasing was noted. The resistance measurements at the DAS termination were entered into the LMS TestLab software package to account for lead wire resistances.

Six data logs were taken for each test condition. Three logs at 10-volt (10V) bridge excitation and three logs at 0-volt (0V) bridge excitation were taken for each power increment. The data logs alternated in the order 10V, 0V, 10V, 0V, 10V, and 0V. The data acquisition time for the 10V and 0V settings were 120 seconds and 40 seconds, respectively. The 10V and 0V log files were measured in immediate succession to identify electrical noise. Prior to each data log the strain gauges were balanced and shunt calibrated.

A data set was defined as a 10V and 0V pair. Maximum, minimum, mean and ranges were calculated for each strain gauge pair. The data was checked for saturation to make sure the data amplitude did not exceed the channel range. Saturation never occurred during testing. Averaged time history data for the strain gauge pairs at each location were calculated along with the averaged PSDs. A maximum PSD value of 250 Hz was saved and plotted. Coherence between the averaged lower and upper strain gauge pairs was also calculated.

Data set one is shown in the Attachment A plots. Data sets two and three were similar to data set one. The averaged plant processed data can be found in Attachment C.

5.2 Primary System Pressurization Test

The strain gauge installation was checked against plant processed data during the primary system pressurization check. As mentioned in Section 4.2 of this appendix, the testing consisted of continuous measurements from zero to full pressure. Then when the primary system pressurization check was complete and the plant was ready to return to ambient pressure, the DAS was nulled and calibrated and continuous measurements were made from full pressure to ambient. The reactor pressure during pressurization went from 14.4 psig to 1027.7 psig. The reactor coolant temperature went from 171°F to 182°F. The reactor pressure during depressurization went from 1032 psig to 17 psig. The reactor coolant temperature during depressurization went from 220°F to 135°F.

5.3 Strain-to-Pressure Conversion

The strain-to-pressure conversion factors were determined using the formula for a thick walled cylinder with closed ends subject to internal pressure only. The conversion factor can be calculated using the following formula:

[[

]]

MSL diameter and thickness UT measurements were taken on September 30, 2008 thru October 2, 2008.

Table 3 below summarizes the conversion factors for each of the [[ ]] strain gauge locations during the hydro test. The Modulus of Elasticity for carbon steels (A516 GR70) as a function of temperature was taken from the ASME Codes (Reference 1).

Table 3. Pipe Dimensions and Strain-to-Pressure Conversion

[[

]]

5.4 Power Ascension Measurements

Attachment A contains the PSD plots for each sensor location at each power level taken during power ascension. Following data collection at each test point, the measured signal data was processed and plotted in the frequency domain for review before ascending to the next power step. The PSD plots represent measurements averaged over 120 seconds of MSL strain data. The PSDs are averaged based on a series of two second long segments, with the adjacent segments overlapping by 50%. The individual strain gauge signals, the averaged strain gauge signals (both excited and non-excited) and coherence between averaged strain gauge signals at the upper and lower sensor locations on the same MSL are plotted on the PSDs. As can be seen in the figures in Attachment A, the individual gauge signals in many frequency bands diverge as a result of the pipe vibration. The black line shows the PSD for the time domain average of the signals for the four pairs of strain gauges. The signals are averaged to define the average hoop strain, which is proportional to the average dynamic pressure at the monitoring location.

Attachment B contains waterfall plots for each sensor location showing the frequency and amplitude content during the power ascension. Attachment C contains the plant operating data at each of the power ascension steps. Attachment D contains the report from the low power measurements taken during RFO-17 to evaluate the noise floor and electrical interference.

5.5 Coherence

Coherence is the measure of the correlation between two signals at a particular frequency. As the coherence approaches a maximum of 1.0 the correlation between the two signals is stronger. When the coherence is 1.0 the two signals are perfectly correlated. When the coherence is zero there is no relationship between the two signals.

Coherence values are included in the PSD plots in Attachment A. The coherence was calculated between the upper and lower strain gauge locations for all steam lines and between the third and lower locations for MSL A and C.

Table 4 is the tabulation of the three highest coherence levels for each power level for frequencies less than approximately 190 Hz and the frequencies at which they occur. The fourth column pair is the coherence peaks in the frequency band from approximately 190-250 Hz. High coherence between measurement locations is indicative of acoustic modes that are being excited in the vessel and MSL system.

Table 4. Coherence in MSL Measurements

[[

]]

6.0 References

1. ASME Boiler and Pressure Vessel Code, Section II, Part D, Subpart 2, Table TM-1, pg. 671.

Attachment A: PSD and Coherence Plots

[[

]]

Figure 11. A-Third PSD and Coherence, 75% CLTP

[[

]]

Figure 12. A-Upper PSD and Coherence, 75% CLTP

[[

]]

Figure 13. A-Lower PSD and Coherence, 75% CLTP

[[

]]

Figure 14. B-Upper PSD and Coherence, 75% CLTP

[[

]]

Figure 15. B-Lower PSD and Coherence, 75% CLTP

[[

]]

Figure 16. C-Upper PSD and Coherence, 75% CLTP

[[

]]

Figure 17. C-Third PSD and Coherence, 75% CLTP

[[

]]

Figure 18. C-Lower PSD and Coherence, 75% CLTP

[[

]]

Figure 19. D-Upper PSD and Coherence, 75% CLTP

[[

]]

Figure 20. D-Lower PSD and Coherence, 75% CLTP

[[

]]

Figure 21. A-Third PSD and Coherence, 80% CLTP

[[

]]

Figure 22. A-Upper PSD and Coherence, 80% CLTP

[[

]]

Figure 23. A-Lower PSD and Coherence, 80% CLTP

[[

]]

Figure 24. B-Upper PSD and Coherence, 80% CLTP

[[

]]

Figure 25. B-Lower PSD and Coherence, 80% CLTP

[[

]]

Figure 26. C-Upper PSD and Coherence, 80% CLTP

[[

]]

Figure 27. C-Third PSD and Coherence, 80% CLTP

[[

]]

Figure 28. C-Lower PSD and Coherence, 80% CLTP

[[

]]

Figure 29. D-Upper PSD and Coherence, 80% CLTP

[[

]]

Figure 30. D-Lower PSD and Coherence, 80% CLTP

[[

]]

Figure 31. A-Third PSD and Coherence, 85% CLTP

[[

]]

Figure 32. A-Upper PSD and Coherence, 85% CLTP

[[

]]

Figure 33. A-Lower PSD and Coherence, 85% CLTP

[[

]]

Figure 34. B-Upper PSD and Coherence, 85% CLTP

[[

]]

Figure 35. B-Lower PSD and Coherence, 85% CLTP

[[

]]

Figure 36. C-Upper PSD and Coherence, 85% CLTP

[[

]]

Figure 37. C-Third PSD and Coherence, 85% CLTP

[[

]]

Figure 38. C-Lower PSD and Coherence, 85% CLTP

[[

]]

Figure 39. D-Upper PSD and Coherence, 85% CLTP

[[

]]

Figure 40. D-Lower PSD and Coherence, 85% CLTP

[[

]]

Figure 41. A-Third PSD and Coherence, 90% CLTP

[[

]]

Figure 42. A-Upper PSD and Coherence, 90% CLTP

[[

]]

Figure 43. A-Lower PSD and Coherence, 90% CLTP

[[

]]

Figure 44. B-Upper PSD and Coherence, 90% CLTP

[[

]]

Figure 45. B-Lower PSD and Coherence, 90% CLTP

[[

]]

Figure 46. C-Upper PSD and Coherence, 90% CLTP

[[

]]

Figure 47. C-Third PSD and Coherence, 90% CLTP

[[

]]

Figure 48. C-Lower PSD and Coherence, 90% CLTP

[[

]]

Figure 49. D-Upper PSD and Coherence, 90% CLTP

[[

]]

Figure 50. D-Lower PSD and Coherence, 90% CLTP

[[

]]

Figure 51. A-Third PSD and Coherence, 95% CLTP

[[

]]

Figure 52. A-Upper PSD and Coherence, 95% CLTP

[[

]]

Figure 53. A-Lower PSD and Coherence, 95% CLTP

[[

]]

Figure 54. B-Upper PSD and Coherence, 95% CLTP

[[

]]

Figure 55. B-Lower PSD and Coherence, 95% CLTP

[[

]]

Figure 56. C-Upper PSD and Coherence, 95% CLTP

[[

]]

Figure 57. C-Third PSD and Coherence, 95% CLTP

[[

]]

Figure 58. C-Lower PSD and Coherence, 95% CLTP

[[

]]

Figure 59. D-Upper PSD and Coherence, 95% CLTP

[[

]]

Figure 60. D-Lower PSD and Coherence, 95% CLTP

[[

]]

Figure 61. A-Third PSD and Coherence, 100% CLTP

[[

]]

Figure 62. A-Upper PSD and Coherence, 100% CLTP

[[

]]

Figure 63. A-Lower PSD and Coherence, 100% CLTP

[[

]]

Figure 64. B-Upper PSD and Coherence, 100% CLTP

[[

]]

Figure 65. B-Lower PSD and Coherence, 100% CLTP

[[

]]

Figure 66. C-Upper PSD and Coherence, 100% CLTP

[[

]]

Figure 67. C-Third PSD and Coherence, 100% CLTP

[[

]]

Figure 68. C-Lower PSD and Coherence, 100% CLTP

[[

]]

Figure 69. D-Upper PSD and Coherence, 100% CLTP

[[

]]

Figure 70. D-Lower PSD and Coherence, 100% CLTP

Attachment B: Waterfall Plots

[[

]]

Figure 71. A-Third Average PSD vs % Power Waterfall Plot

[[

]]

Figure 72. A-Upper Average PSD vs % Power Waterfall Plot

[[

]]

Figure 73. A-Lower Average PSD vs % Power Waterfall Plot

[[

]]

Figure 74. B-Upper Average PSD vs % Power Waterfall Plot

[[

]]

Figure 75. B-Lower Average PSD vs % Power Waterfall Plot

[[

]]

Figure 76. C-Upper Average PSD vs % Power Waterfall Plot

[[

]]

Figure 77. C-Third Average PSD vs % Power Waterfall Plot

[[

]]

Figure 78. C-Lower Average PSD vs % Power Waterfall Plot

[[

]]

Figure 79. D-Upper Average PSD vs % Power Waterfall Plot

[[

]]

Figure 80. D-Lower Average PSD vs % Power Waterfall Plot

Attachment C: Plant Data

[[

]]

[[

]]

[[

]]

[[

]]

Attachment D: Grand Gulf Nuclear Station Main Steam Line Low Power Measurement Report

D1.0 Purpose

The purpose of this attachment is to provide the results of the data acquisition and initial analysis from the MSLs at the GGNS during RFO-17. Strain gauges mounted on the surface of the MSLs within the drywell were used to measure the dynamic pressure waves during power ascension at low power levels. This data will be used to evaluate the signal noise floor and interference not visible in higher power data.

D2.0 Instrumentation

D2.1 Sensor Installation

The original strain gauge installation during RFO-16 was done in Sept.-Oct. 2008. During RFO-17 in May 2010, these strain gauges were used to measure static and dynamic signals to evaluate the noise floor level and electrical and mechanical noise at low power levels. The installation locations and procedure used during RFO-16 are described in Section 3 of this attachment.

D2.2 Data Acquisition System

The DAS was located on a cart inside the auxiliary building at elevation 139'. It consisted of the LMS SCADAS Mobile unit, 700-Ohm resistor bridge completion box, data acquisition laptop computer and analysis laptop computer. Signal conditioning for the strain gauges was contained in the LMS SCADAS modules. An isolation transformer was placed between the DAS and the plant AC power to provide clean power to the acquisition system. A photo of the DAS setup inside the auxiliary building can be seen in Figure 9 of this appendix.

D3.0 Tests Performed

D3.1 System Checkout

Resistance measurements were made to establish the survival rate of the strain gauges since installation in 2008. From these measurements, it was determined that a majority of the strain gauges had survived. These measurements indicated that five channels had changed in resistance by more than 10%. Upon arrival on site, these measurements were repeated with similar results. To improve the ability of the data acquisition system to balance, resistors were added in the bridge completion box to bring the arms of the bridge closer together. Channels [[ ]] had resistors added.

D3.2 Sensor Pre-Calibration

During RFO-16 it was concluded that two channels were unusable, [[ ]]. These channels were turned off during data acquisition in 2008.

For RFO-17, the sensors were pre-calibrated on May 20, 2010 at the GGNS through the LMS DAS. During calibration, the DAS was not able to stabilize two channels. These channels, [[ ]], were turned off and not used in the data acquisition. [[ ]] original channels were used throughout the testing.

D3.3 Primary System Pressurization Test

After the sensor pre-calibration, the strain gauges were measured statically during the Primary System Pressurization Test on May 20-21, 2010. Transient records during pressurization and de-pressurization conditions were recorded. The static strain levels were then converted to equivalent pressure using the MSL dimensions and compared with plant pressure instrumentation.

D3.4 Power Ascension

Steady state power conditions were used to measure the fluctuating pressure in the MSLs. Measurements were taken at [[
]]. Power ascension data was taken from May 26, 2010 to May 27, 2010.

D3.5 Sensor Post-Calibration

The sensors were post-calibrated on May 28, 2010 with the LMS DAS. [[ ]] channels were found to be out of tolerance during the Post Cal Checkout. Data from these sensors was not used for the analysis.

D4.0 Data Acquisition Analysis

D4.1 Data Acquisition and Analysis Process

The MSL vibration data was collected with a laptop computer and a LMS SCADAS Mobile unit using a sampling frequency of [[ ]]. The resistance measurements at the DAS termination were entered into the LMS TestLab software package to account for lead wire resistances.

Six data logs were taken for each test condition. Three logs at 10V bridge excitation and three logs at 0V bridge excitation were taken for each power increment. The data logs alternated in the order 10V, 0V, 10V, 0V, 10V and 0V. The data acquisition time for the 10V and 0V settings were 120 seconds and 40 seconds, respectively. The 10V and 0V log files were measured in immediate succession to identify electrical noise. In the third set an additional 0V without nulling was performed. Prior to each data log the strain gauges were balanced and shunt calibrated.

A data set was defined as a 10V and 0V pair. The entire unfiltered data log was evaluated. Maximum, minimum, mean and ranges were calculated for each strain gauge pair. The data was checked for saturation to make sure the data amplitude did not exceed the channel range. Saturation never occurred during testing. Averaged time history data for the strain gauge pairs at each location were calculated along with the averaged PSDs. A maximum PSD value of 250 Hz was saved and plotted. Coherence between the averaged lower and upper strain gauge pairs was also calculated.

Data set one is shown in the attachment plots. Data sets two and three were similar to data set one.

D4.2 Primary System Pressurization Test

The strain gauge installation was checked against plant-processed data during the primary system pressurization check. As mentioned in Section D3.3, data was recorded during both pressurization and depressurization. The DAS was nulled and calibrated and continuous measurements were made from zero to full pressure. When the primary system pressurization check was complete and the plant was ready to return to ambient pressure, the DAS was nulled and calibrated and continuous measurements were made from full pressure to ambient. The reactor pressure during pressurization went from 6.7 psig to 1023.5 psig. The reactor pressure during depressurization went from 1027.7 psig to 20.1 psig.

D4.3 Noise Analysis

Measurements at 0V bridge excitation were taken for each test condition. The average 0V PSD data is included in the attachment plots. Comparing this measurement with the 10V average PSD data indicates the noise floor and points out potential electrical or mechanical

noise in the measurement. Table 1D below shows the noise frequencies at each power level identified by this measurement. These potential noise frequencies appear across all measurement channels at the specified power levels.

Table 1D. Measurement Noise Frequencies

Power level	Noise Frequencies (Hz)		
[[			
			]]

The 60Hz and 180Hz are typical electrical noise from the line frequency (and higher harmonics). There is other noise that only appeared on the channels for the Lower B and Lower D strain gauges. The identified frequencies are shown in Table 2D. Below 30% CLTP the recirculation pumps were operating at low speed, corresponding to a drive frequency of 15 Hz. Above 30% CLTP they are switched to high speed. At high speed the recirculation pumps were operating at a drive frequency of 60 Hz. At high speed the recirculation pumps are operating at about 1793 rpm (Pump A – 1789 rpm, Pump B – 1797 rpm). This would correspond to a rotational frequency of 29.8 Hz. The 149 Hz corresponds to a fifth harmonic of the rotational frequency. These pumps have a five-vane impeller. The vane passing frequency for a five-vane impeller at 1793 rpm is 149 Hz. Because the recirculation pump motors are induction motors, this electrical interference could be induced by the pressure resistance as the impeller blade passes the cutwater. The momentary slowing of the blade increases the rotor's field strength to handle the extra load. This would then feed back into the current on the bus, where it would show up as electrical interference that is synchronized with the vane passing frequency.

Table 2D. Local Noise Frequencies

Power Level	Noise Frequencies (Hz)
[[	
	]]

Figures 1D through 10D show waterfall plots of the 0V noise for each strain gauge location. Figures 11D through 30D show PSD plots of locations where an orthogonal set of strain gauges produced quality data. Other locations had two sets of quality strain gauges but these were not an orthogonal pair and are not shown here.

[[

]]

Figure 1D. A-Third 0V Average PSD vs % Power Waterfall Plot

[[

]]

Figure 2D. A-Upper 0V Average PSD vs % Power Waterfall Plot

[[

]]

Figure 3D. A-Lower 0V Average PSD vs % Power Waterfall Plot

[[

]]

Figure 4D. B-Upper 0V Average PSD vs % Power Waterfall Plot

[[

]]

Figure 5D. B-Lower 0V Average PSD vs % Power Waterfall Plot

[[

]]

Figure 6D. C-Upper 0V Average PSD vs % Power Waterfall Plot

[[

]]

Figure 7D. C-Third 0V Average PSD vs % Power Waterfall Plot

[[

]]

Figure 8D. C-Lower 0V Average PSD vs % Power Waterfall Plot

[[

]]

Figure 9D. D-Upper 0V Average PSD vs % Power Waterfall Plot

[[

]]

Figure 10D. D-Lower 0V Average PSD vs % Power Waterfall Plot

[[

]]

Figure 11D. B-Upper Average PSD and Coherence, 10% CLTP

[[

]]

Figure 12D. B-Lower Average PSD and Coherence, 10% CLTP

[[

]]

Figure 13D. C-Lower Average PSD and Coherence, 10% CLTP

[[

]]

Figure 14D. D-Lower Average PSD and Coherence, 10% CLTP

[[

]]

Figure 15D. B-Upper Average PSD and Coherence, 20% CLTP

[[

]]

Figure 16D. B-Lower Average PSD and Coherence, 20% CLTP

[[

]]

Figure 17D. C-Lower Average PSD and Coherence, 20% CLTP

[[

]]

Figure 18D. D-Lower Average PSD and Coherence, 20% CLTP

[[

]]

Figure 19D. B-Upper Average PSD and Coherence, 24% CLTP

[[

]]

Figure 20D. B-Lower Average PSD and Coherence, 24% CLTP

[[

]]

Figure 21D. C-Lower Average PSD and Coherence, 24% CLTP

[[

]]

Figure 22D. D-Lower Average PSD and Coherence, 24% CLTP

[[

]]

Figure 23D. B-Upper Average PSD and Coherence, 40% CLTP

[[

]]

Figure 24D. B-Lower Average PSD and Coherence, 40% CLTP

[[

]]

Figure 25D. C-Lower Average PSD and Coherence, 40% CLTP

[[

]]

Figure 26D. D-Lower Average PSD and Coherence, 40% CLTP

[[

]]

Figure 27D. B-Upper Average PSD and Coherence, 50% CLTP

[[

]]

Figure 28D. B-Lower Average PSD and Coherence, 50% CLTP

[[

]]

Figure 29D. C-Lower Average PSD and Coherence, 50% CLTP

[[

]]

Figure 30D. D-Lower Average PSD and Coherence, 50% CLTP